



UNIVERSITY OF LEEDS

This is a repository copy of *Impact of Changes to the Atmospheric Soluble Iron Deposition Flux on Ocean Biogeochemical Cycles in the Anthropocene*.

White Rose Research Online URL for this paper:

<http://eprints.whiterose.ac.uk/160674/>

Version: Published Version

---

**Article:**

Hamilton, DS, Moore, JK, Arneth, A et al. (10 more authors) (2020) Impact of Changes to the Atmospheric Soluble Iron Deposition Flux on Ocean Biogeochemical Cycles in the Anthropocene. *Global Biogeochemical Cycles*, 34 (3). e2019GB006448. ISSN 0886-6236

<https://doi.org/10.1029/2019gb006448>

---

©2020. American Geophysical Union. All Rights Reserved. Reproduced in accordance with the publisher's self-archiving policy.

**Reuse**

Items deposited in White Rose Research Online are protected by copyright, with all rights reserved unless indicated otherwise. They may be downloaded and/or printed for private study, or other acts as permitted by national copyright laws. The publisher or other rights holders may allow further reproduction and re-use of the full text version. This is indicated by the licence information on the White Rose Research Online record for the item.

**Takedown**

If you consider content in White Rose Research Online to be in breach of UK law, please notify us by emailing [eprints@whiterose.ac.uk](mailto:eprints@whiterose.ac.uk) including the URL of the record and the reason for the withdrawal request.



# Global Biogeochemical Cycles

## RESEARCH ARTICLE

10.1029/2019GB006448

### Key Points:

- Human activity significantly modifies the magnitude and location of atmospheric soluble iron deposition to the oceans
- Marine carbon cycle responses to Anthropocene iron flux changes are modest but more sensitive to varying fire than dust iron emissions
- Increasing the iron flux produces offsetting patterns in phytoplankton macronutrient uptake and productivity rates at the basin scale

### Supporting Information:

- Supporting Information S1

### Correspondence to:

D. S. Hamilton,  
dsh224@cornell.edu

### Citation:

Hamilton, D. S., Moore, J. K., Arnett, A., Bond, T. C., Carslaw, K. S., Hantson, S., et al. (2020). Impact of changes to the atmospheric soluble iron deposition flux on ocean biogeochemical cycles in the Anthropocene. *Global Biogeochemical Cycles*, 34, e2019GB006448. <https://doi.org/10.1029/2019GB006448>

Received 9 OCT 2019

Accepted 16 FEB 2020

Accepted article online 20 FEB 2020

## Impact of Changes to the Atmospheric Soluble Iron Deposition Flux on Ocean Biogeochemical Cycles in the Anthropocene

Douglas S. Hamilton<sup>1</sup> , J. Keith Moore<sup>2</sup>, Almut Arnett<sup>3</sup>, Tami C. Bond<sup>4</sup>, Ken S. Carslaw<sup>5</sup> , Stijn Hantson<sup>6</sup> , Akinori Ito<sup>7</sup> , Jed O. Kaplan<sup>8</sup>, Keith Lindsay<sup>9</sup>, Lars Nieradzik<sup>10</sup>, Sagar D. Rathod<sup>11</sup> , Rachel A. Scanza<sup>12</sup>, and Natalie M. Mahowald<sup>1</sup>

<sup>1</sup>Department of Earth and Atmospheric Science, Cornell University, Ithaca, NY, USA, <sup>2</sup>Department of Earth System Science, University of California, Irvine, CA, USA, <sup>3</sup>Institute of Meteorology and Climate Research/Atmospheric Environmental Research, Karlsruhe Institute of Technology, Garmisch-Partenkirchen, Germany, <sup>4</sup>Department of Mechanical Engineering, Colorado State University, Fort Collins, CO, USA, <sup>5</sup>School of Earth and Environment, University of Leeds, Leeds, UK, <sup>6</sup>Geospatial Data Solutions Center, University of California, Irvine, CA, USA, <sup>7</sup>Yokohama Institute for Earth Sciences, JAMSTEC, Yokohama, Japan, <sup>8</sup>Department of Earth Sciences, The University of Hong Kong, Hong Kong, <sup>9</sup>National Center for Atmospheric Research, Boulder, CO, USA, <sup>10</sup>Institute for Physical Geography and Ecosystem Sciences, Lund University, Lund, Sweden, <sup>11</sup>Department of Atmospheric Science, Colorado State University, Fort Collins, CO, USA, <sup>12</sup>Atmospheric Sciences and Global Change Division, Pacific Northwest National Laboratory, Richland, WA, USA

**Abstract** Iron can be a growth-limiting nutrient for phytoplankton, modifying rates of net primary production, nitrogen fixation, and carbon export - highlighting the importance of new iron inputs from the atmosphere. The bioavailable iron fraction depends on the emission source and the dissolution during transport. The impacts of anthropogenic combustion and land use change on emissions from industrial, domestic, shipping, desert, and wildfire sources suggest that Northern Hemisphere soluble iron deposition has likely been enhanced between 2% and 68% over the Industrial Era. If policy and climate follow the intermediate Representative Concentration Pathway 4.5 trajectory, then results suggest that Southern Ocean (>30°S) soluble iron deposition would be enhanced between 63% and 95% by 2100. Marine net primary productivity and carbon export within the open ocean are most sensitive to changes in soluble iron deposition in the Southern Hemisphere; this is predominantly driven by fire rather than dust iron sources. Changes in iron deposition cause large perturbations to the marine nitrogen cycle, up to 70% increase in denitrification and 15% increase in nitrogen fixation, but only modestly impacts the carbon cycle and atmospheric CO<sub>2</sub> concentrations (1–3 ppm). Regionally, primary productivity increases due to increased iron deposition are often compensated by offsetting decreases downstream corresponding to equivalent changes in the rate of phytoplankton macronutrient uptake, particularly in the equatorial Pacific. These effects are weaker in the Southern Ocean, suggesting that changes in iron deposition in this region dominates the global carbon cycle and climate response.

## 1. Introduction

Human activity alters the magnitude of the atmospheric aerosol metal flux to the oceans (Mahowald et al., 2018), mainly through the following: increasing the combustion of fossil fuels for industrial, transportation, and domestic purposes; altering land cover distributions through practices such as deforestation and urbanization or agricultural and pastoral land use; and altering atmospheric concentrations of acidic and organic species (which increase metal solubility during transport). Understanding how human activity modifies the atmospheric fluxes of metals to the oceans is important due to the impact of the deposited metals on the growth and development of the phytoplankton community (Boyd et al., 2017; Jickells et al., 2005; Mahowald et al., 2018; Moore, Mills, et al., 2013) and thus their potential to enhance carbon sinks. While deposition of metals such as iron, zinc, and manganese are beneficial for phytoplankton (Morel & Price, 2003; Wyatt et al., 2014), other metals such as copper are toxic at high concentrations (Jordi et al., 2012; Paytan et al., 2009; Zhang et al., 2019). Due to iron's critical role as a micronutrient required by ocean biota for primary productivity (Martin, 1990; Martin et al., 1991; Tagliabue et al., 2017), here we focus on how

human activity alters the magnitude of atmospheric soluble iron deposition to the oceans and diagnose the resulting impact on ocean biogeochemistry. Changes to other oceanic sources of iron, such as hydrothermal vents or sedimentary and riverine inputs (e.g., Tagliabue et al., 2017), are not diagnosed in this study but are thought to be less likely to be altered by human activity in the Anthropocene (Hutchins & Boyd, 2016).

There is evidence that anthropogenic activity over the Industrial Era up to doubled mineral dust aerosol emissions (Mahowald et al., 2010) and halved wildfire and agricultural burning aerosol emissions (Hamilton et al., 2018). It is therefore likely that a strong anthropogenic perturbation to natural aerosol emissions has occurred over the last two-to-three centuries. Over the same period, aerosol emissions from industrial, domestic, and shipping sources rose exponentially (Bond et al., 2007; Ito & Penner, 2005). Mineral dust, fires, and anthropogenic combustion emissions carry metallic aerosols, especially iron (Chuang et al., 2005; Guieu et al., 2005; Mahowald et al., 2009; Rauch & Pacyna, 2009); therefore, the atmospheric burden and ocean deposition of metals is synchronized with human activity during the Anthropocene.

Large areas of the world's oceans are rich in macronutrients, yet phytoplankton growth rates remain low even under well-stratified conditions. Mesoscale fertilization experiments conducted *in situ* within these high-nutrient, low-chlorophyll (HNLC) regions have demonstrated that iron addition increases phytoplankton growth rates and biological biomass accumulation (Boyd et al., 2007; de Baar et al., 2005). In warm, oligotrophic regions, diazotrophic, or nitrogen-fixing, phytoplankton are often limited by iron availability, although the larger community may be nitrogen or phosphorus limited. Nitrogen fixed by diazotrophs eventually becomes available to the larger community, often reducing nitrogen stress. Thus, iron deposition can influence biological carbon export (the biological pump) by directly modifying community iron stress in the HNLC regions and indirectly in the oligotrophic regions (containing low nutrient concentrations) by modifying rates of nitrogen fixation (Capone et al., 1997; Falkowski, 1997; Moore et al., 2006). Due to its key role in the ocean biological pump, iron deposition modulates ocean biogeochemistry (Boyd et al., 2017; Jickells et al., 2005; Moore et al., 2006) with significant changes in the magnitude of iron deposition fluxes altering ocean-atmosphere CO<sub>2</sub> exchange rates and impacting climate (Martin, 1990).

By 2000, human land use and land cover change transformed more than 70% of the Earth's terrestrial biomes from wildlands to seminatural and active anthromes (human land cover types), with significant transformations having occurred post 1700 (Ellis et al., 2010, 2013). Human activity on this scale increases dust emissions in many environments (Brown et al., 2017; Ginoux et al., 2012; McConnell et al., 2007; Mulitz et al., 2010; Neff et al., 2008; Stanelle et al., 2014), and thus iron emissions, as mineral dust contains ~3.5% iron by mass (Jickells et al., 2005; Shi et al., 2012). While dust is the dominant (>90%) source of total aerosol bearing iron to the open ocean (Mahowald et al., 2009), a secondary source of iron comes from pyrogenic sources, including vegetation fires (Guieu et al., 2005; Ito, 2011; Paris et al., 2010; Winton et al., 2015), industrial and domestic combustion (Chen et al., 2012; Chuang et al., 2005; Luo et al., 2008; Myriokefalitakis et al., 2015), and shipping emissions (Ito, 2013). However, significant differences exist in the particle size distribution and oxidation state of iron between dust and pyrogenic sources, and thus the soluble iron fraction also differs (i.e., the ratio of water leachable iron to total iron, often considered the bioavailable fraction) (Baker & Croot, 2010; Schroth et al., 2009; Shi et al., 2012). Specifically, larger mineral dust particles generally have a low (<0.5%) iron soluble fraction at deposition (Chen & Siefert, 2003; Hand et al., 2004; Sholkovitz et al., 2012) and contain substantial minerals with strong iron-oxygen bonds (e.g., hematite and goethite), while smaller pyrogenic particles have a higher (18–81%) iron soluble fraction at emission (Bowie et al., 2009; Chen et al., 2012; Oakes et al., 2012; Schroth et al., 2009) and contain substantially more labile minerals (e.g., ferric sulfates) than mineral dust.

Once airborne, acidic (Li et al., 2017; Meskhidze et al., 2003; Oakes et al., 2012; Shi et al., 2015; Solmon et al., 2009) and water-soluble organic (Ito, 2015; Johnson & Meskhidze, 2013; Myriokefalitakis et al., 2015) gaseous (and aerosol) species from biological and combustion sources readily condense onto (and coagulate with) iron-bearing aerosol. During atmospheric transport the iron oxidation state can then reduce photochemically by acidic and organic ligand (e.g., oxalate) processing, enhancing the soluble iron fraction (Li et al., 2017; Sedwick et al., 2007; Solmon et al., 2009). As fossil fuel combustion, fires, and biogenic activity emit oxalate directly or indirectly via its precursor gases, regional changes in the rate of atmospheric

dissolution of iron via organic ligand complexation could be impacted by human activity. Acidic and organic gas emissions from industry and vegetation are colocated with pyrogenic iron aerosol emissions (Myriokefalitakis et al., 2011; Oakes et al., 2012). However, mineral dust sources are located further away from industry and vegetation and so it takes longer for dust iron aerosol to encounter and mix with acidic and organic compounds. Thus, dust aerosol can be expected in general to be less mixed with acidic and organic iron processing species compared to pyrogenic iron aerosol which are mixed in-plume at the point of emission. Additionally, smaller pyrogenic particles tend to have longer lifetimes (Textor et al., 2006) and thus even with the same rate of solubilization will become more soluble in the atmosphere (Hand et al., 2004). Furthermore, as dust contains a significant fraction of carbonate, a pH buffer (Böke et al., 1999), aerosol acidity will be initially neutralized, further reducing mineral dust iron dissolution rates compared to its pyrogenic iron counterpart (Ito et al., 2019).

Changes to the magnitude of soluble iron deposition is hypothesized to alter global biogeochemical cycles, and hence the carbon cycle, across glacial-interglacial timescales (Kohfeld & Ridgwell, 2009; Martin, 1990). However, the impacts of human activity on the iron cycle through rapid industrialization and land use change since the beginning of the Industrial Revolution (ca. 1750 CE) is less well known, although large effects have previously been suggested (Aumont et al., 2008; Bopp et al., 2013; Mahowald, Lindsay, et al., 2011, 2010; Tagliabue et al., 2008, 2009). Here we use monthly mean output of atmospheric soluble iron deposition from a global aerosol model including atmospheric processing of iron (Scanza et al., 2015, 2018) as the input to a detailed ocean biogeochemistry model (Moore et al., 2004, Moore, Lindsay, et al., 2013). We consider how anthropogenic activity perturbs the magnitude of iron emissions through the following: the impact of land use and land cover change on wildfire and dust emissions; increasing industrial combustion emissions; population increases on domestic combustion emissions; and increasing shipping emissions. We also consider how changes in atmospheric chemistry (via industrialization) alters the atmospheric processing (aerosol pH and oxalate) of iron to a soluble (bioavailable) form during transport. For the first time, we specifically consider how changes in wildfires, dust, anthropogenic (industrial, domestic, and shipping) combustion emissions, and atmospheric iron processing from the past (ca. 1750 CE) to the future (ca. 2100 CE) are separately and collectively impacting ocean biogeochemistry via changes in the magnitude of the atmospheric soluble iron deposition flux.

## 2. Methods

The modeled ocean biogeochemistry response to anthropogenically mediated changes in the atmospheric deposition of soluble iron was simulated for aerosol emissions and an atmospheric state representative of three time periods: preindustrial (PI; ca. 1750 CE), present day (PD; ca. 2008 CE), and the future (FU; ca. 2100 CE). A total of six cases (three base simulations, PIBASE, PDBASE, and FUBASE, and three sensitivity simulations, PIHIGHDUST, PIHIGHCOMB, and PDHIGHCOMB) quantified the range in atmospheric emissions of iron and its solubilization during transport within a global aerosol model (Table 1; parameter value justifications within section 2). A detailed ocean biogeochemistry model then quantified the response of the marine carbon and nitrogen cycles to the diagnosed range of soluble iron deposition to the ocean. For all simulations, climate forcings and other iron sources to the ocean were held constant to isolate the impact of anthropogenic changes to the atmospheric soluble iron flux on ocean biogeochemistry, via perturbing the “natural” iron cycle.

### 2.1. Aerosol Model

We used the Community Atmosphere Model version 4 (CAM4), within the National Center for Atmospheric Research Community Earth System Model (CESM) version 1.0.5 (CESM 1.0.5), with a  $2.5^\circ \times 1.9^\circ$  horizontal resolution and 56 vertical layers up to 2 hPa (Hurrell et al., 2013). Meteorology in all time periods was forced to NASA's GEOS-5 reanalysis data set (Rienecker et al., 2008) for 2005–2011, with the first year discarded as a “spin-up period” and the mean of the last 5 years used for analysis.

Desert dust was modeled via the Dust Entrainment and Deposition module (Zender, 2003), previously updated to include information on dust mineralogy (illite, kaolinite, smectite, feldspar, calcite, and hematite; Scanza et al., 2015) and mineral size fractions (Kok, 2011; Scanza et al., 2018). In total, six tracers of iron were advected within each of the four CAM4 size bins (0.1–1, 1–2.5, 2.5–5.0, and 5.0–10  $\mu\text{m}$ ): medium reactive

**Table 1**

Preindustrial (PI; ca. 1750 CE), Present Day (PD; ca. 2008 CE), and Future (FU; ca. 2100 CE) Emission Specification for Dust, Fires, Domestic Biofuel, Industrial Combustion, and Shipping in Each Simulated Case

Case	Dust	Fires	Domestic (biofuel and coal)	Industrial (wood, coal, and oil)	Shipping (oil and diesel)
PIBASE	1880	SIMFIRE-BLAZE 1750	1750 (10% Fe solubility)	—	—
PIHIGHDUST	2006– 2010	SIMFIRE-BLAZE 1750	1750 (10% Fe solubility)	—	—
PIHIGHCOMB	1880	LMfire 1770	20% PD (4% Fe solubility)	20% PD (4% Fe solubility)	—
PDBASE	2006– 2010	SIMFIRE-BLAZE 2008	PD (4% Fe solubility)	PD (4% Fe solubility)	2006 (36% Fe solubility)
PDHIGHCOMB	2006– 2010	SIMFIRE-BLAZE 2008	PD × 5 (4% Fe solubility)	PD × 5 (4% Fe solubility)	2006 (79% Fe solubility)
FUBASE	2100 <sup>a</sup>	RCP4.5	PD × 5 × (FU:PD BC) (4% Fe solubility)	PD × 5 × (FU:PD BC) (4% Fe solubility)	2006 × 1.65 (79% Fe solubility)

Note. Future anthropogenic emission changes were calculated using the FU (Representative Concentration Pathway 4.5; RCP4.5) to PD (AeroCom; Dentener et al., 2006) ratio in black carbon (BC) emissions. Future fire, domestic, and industrial combustion emission changes were calculated per grid cell, while shipping iron emission changes were calculated using a global mean shipping BC change (uniform 65% increase from PD to FU). Industrial combustion includes coal, oil, and wood combustion for power and process heat generation. Domestic combustion for residential cookstoves and space-heating purposes is globally dominated by biofuels such as wood and cow dung, but regionally coal combustion may also be important. We do not account for other possible petroleum emissions of iron (e.g., Wang et al., 2015), which are a minor contributor to oceanic soluble iron deposition compared to shipping. PIBASE = PI dust (Mahowald et al., 2010; Scanza et al., 2018), fires (Hamilton et al., 2018, 2019), and anthropogenic (domestic wood burning only; see section 2) emissions; PIHIGHDUST = PIBASE but PD dust (Scanza et al., 2018) emissions; PIHIGHCOMB = PIBASE but higher fires (approximately doubling; Hamilton et al., 2018) + 20% PD anthropogenic (Scanza et al., 2018) emissions; PDBASE = PD dust, fires, and anthropogenic (Hamilton et al., 2019; Scanza et al., 2018) emissions; PDHIGHCOMB = PDBASE but anthropogenic ×5 PDBASE (Matsui et al., 2018) emissions; FUBASE = RCP4.5 fires and anthropogenic (Ward et al., 2012) emissions.

<sup>a</sup>In the FU case we use PD emissions and multiply deposition with multimodel estimates of future changes following Mahowald (2007).

total and soluble mineral dust iron, slow reactive total and soluble mineral dust iron, and medium reactive combustion total and soluble iron.

Fire aerosol emissions for PI and PD (10-year mean centered on 2008) were supplied from simulations using the LPI-GUESS-SIMFIRE-BLAZE (SIMFIRE-BLAZE herein) fire model (Knorr et al., 2014; Rabin et al., 2017), as reported by Hamilton et al. (2018). An additional regional model observation bias correction factor was applied to fire emissions of black carbon (BC), organic carbon, and sulfur dioxide (supporting information Figure S1), reducing annual mean BC emissions by 2% in the PD (2.10 to 2.06 Tg a<sup>-1</sup>) and increased them by 5% in the PI (3.10 to 3.14 Tg a<sup>-1</sup>) from their original levels. The 19 regional bias correction factors were calculated as the annual mean (2003–2011) ratio of observed mean fire emissions from all three major fire emission databases (The Global Fire Emissions Database: GFED4, The Global Fire Assimilation System: GFAS, and the Fire INventory from NCAR: FINN) to SIMFIRE-BLAZE emissions within each fire region. Fire regions were based on GFED definitions (Giglio et al., 2010), but with an additional subdivision of the United States, Australia, Europe, South America, and boreal Asia regions. Due to the large uncertainty in the magnitude of historical fire emissions (Li et al., 2019), a second PI fire emissions data set using the LMfire model (Pfeiffer et al., 2013) provided an upper limit to fire emissions following the analysis by Hamilton et al. (2018) based on comparisons with paleoenvironmental archives of fire changes (e.g., ice cores and charcoal records). Our high LMfire emissions are approximately double those of SIMFIRE-BLAZE (6.34 vs 3.14 Tg BC a<sup>-1</sup>, respectively). All other aerosol and precursor gas emissions in the PI and PD were taken from Dentener et al. (2006). For the FUBASE simulation fire emissions followed the intermediate Representative Concentration Pathway “RCP4.5” scenario, as calculated using a coupled land carbon model with fire and land use impacts by Ward et al. (2012), and are 5.52 Tg BC a<sup>-1</sup>.

**Table 2**

Mineral Dust and Iron Emissions (Tg yr<sup>-1</sup>) for Each Iron Source at Each Investigated Time Period: Preindustrial (PI; ca. 1750 CE), Present Day (PD; ca. 2008 CE), and Future (FU; ca. 2100 CE)

	Total emissions/Tg a <sup>-1</sup>			Multimodel (PD only)
	PI	PD	FU	
Mineral dust	1,112	1,775	1,775 <sup>a</sup>	—
Dust iron	36	57	57 <sup>a</sup>	38–130
Pyrogenic iron (fire +anthro.)	1.5–2.8	1.6– 4.3	4.7 2.3	1.8–12
Fire iron	1.5–2.7	0.94	2.3	—
Anthropogenic iron	0.7 × 10 <sup>-3</sup> – 0.13	0.68– 3.4	2.4	—

Note. Multimodel range in PD iron emissions includes results from five iron models (Myriokefalitakis et al., 2018; Wang et al., 2015).

<sup>a</sup>In the FU case we use PD emissions and multiply deposition with multimodel estimates of the change by Mahowald (2007).

## 2.2. Preindustrial, Present Day, and Future Iron Emissions

The range of iron emissions from PI to FU in this study (Table 2) reflects current uncertainties in the anthropogenic influence on the three examined iron emission sources within the Anthropocene: mineral dust, fires,

and anthropogenic combustion (Table 1). This range is smaller than the multimodel range (Myriokefalitakis et al., 2018; Wang et al., 2015) for other iron models, caused by structural differences in each models representation of the PD iron cycle. Detailed modeled comparisons of iron concentrations and its soluble fraction with observations and other iron models were previously conducted by Scanza et al. (2018), Myriokefalitakis et al. (2018), and Ito et al. (2019).

### 2.2.1. Mineral Dust Iron Emissions

In each period, the total and soluble iron fraction of each dust mineral (Table S1) was prescribed at emission within the dust module (Ito & Xu, 2014; Journet et al., 2008). This allows the simulation of the mineralogical fraction and the iron fraction within dust (Scanza et al., 2018; Zhang et al., 2015) and has been shown to improve the comparison with observations for iron and minerals, rather than assuming a globally constant fraction (Scanza et al., 2018; Zhang et al., 2015).

There are limited paleo-observations that constrain changes in desert dust between current and preindustrial (Mahowald et al., 2010). Previous estimates of the fraction of PD dust attributable to human activity range from 20% to 50% (Ginoux et al., 2012; Mahowald et al., 2010; Stanelle et al., 2014), and here we estimated a 37% increase following Scanza et al.'s (2018) methodology which incorporated information from limited paleodust records (Mahowald et al., 2010). An upper PI bound in dust emissions is estimated by replacing PI with PD dust emissions (i.e., the impact of climate and land use/cover change on dust emissions becomes zero), resulting in a range of PI mineral dust iron emissions from 36 to 57 Tg Fe  $a^{-1}$  in the PIBASE and PIHIGHDUST scenarios, respectively.

Future emissions of dust are similarly highly uncertain (e.g., Ginoux et al., 2012; Kok et al., 2014; Luo et al., 2003; Mahowald, 2007; Tegen et al., 2004; Woodward et al., 2005). Climate change is a strong driving mechanism for changes in desert dust sources. In order to estimate FU dust deposition, and its soluble iron mass content, we scaled the simulated deposition flux using estimated FU:PD deposition ratios at each grid box, similar to Mahowald et al. (2010). For each of seven dust source areas (North Africa, Middle East, China/Mongolia, North America, South America, Southern Africa, and Australia, Figure 2; Mahowald, 2007) a ratio of the change in desert area was calculated based on simulations of the BIOME4 model (Kaplan et al., 2003) forced with anomalies in temperature, cloudiness, and precipitation from the third Climate Model Intercomparison Project (CMIP3) for 17 climate models, and the mean change in desert area under a no-CO<sub>2</sub> fertilization assumption is used (Mahowald, 2007). We used the no-CO<sub>2</sub> fertilization estimates in the future, since for the change from preindustrial to current, these changes are more consistent with the few paleo-observations available showing an increase in desert dust deposition (e.g., Mahowald et al., 2010). To obtain the estimate of the source-receptor relationship (i.e., the relationship between the dust generated in each source region to the final aerosol deposition grid box location), we used simulations from Mahowald et al. (2010) for source apportionment. Thus, we obtained an estimate of the change in dust deposition fluxes at each grid box for the future, based on a multiple model simulation synthesis of climate change impacts on desert source area size.

### 2.2.2. Pyrogenic Iron Emissions

Following Luo et al. (2008), we used observed Fe:BC mass ratios, recently updated to include information from multiple terrestrial biomes by Hamilton et al. (2019), to estimate fine (<1.0  $\mu m$ ) and coarse (>1.0  $\mu m$ ) iron emissions from fires. Note that the Fe:BC ratio is temporally constant and thus does not account for potential changes in fire regime properties (e.g., flaming vs. smoldering) due to a changing climate (Ito, 2011).

For the PIBASE simulation we assumed no industrial activity or shipping combustion emissions in the PI, leaving only a small domestic biofuel iron aerosol emission source (Dentener et al., 2006). The dominant domestic fuel consumed in the PI was wood (Bond et al., 2007; Fernandes et al., 2007) and assumed here to be only emitting PM1 (>90% by mass; Kleeman et al., 1999; Zhang et al., 2012). An emission factor of 3.5 g[PM1]/kg[wood] consumed (Jayaratne et al., 2018; Li et al., 2009) was used to estimate 1850 country-wise biofuel emissions (Bond et al., 2007) and subsequently scaled back to 1750 based on human population change estimates (Klein Goldewijk et al., 2017). Total iron emissions are then based on an assumed iron mass fraction (0.04) in combustion PM1 (Alves et al., 2011; Schmidl et al., 2008; Watson & Chow, 2001; Zhang et al., 2012). For the PIHIGHCOMB scenario we followed Scanza et al. (2018) where estimates of PI iron emissions from industrial activity were assumed to scale linearly with the historical

industrial BC emissions reported by Lamarque et al. (2010) for CMIP5, resulting in PIHIGHCOMB anthropogenic combustion emissions being 20% of PDBASE levels ( $0.13 \text{ Tg Fe a}^{-1}$ ).

Anthropogenic combustion PD iron emissions are those reported by Luo et al. (2008), where 4% of iron is assumed to be soluble at emission. To this we added shipping emissions of iron based on the iron content and emissions of particulate matters (Ito et al., 2018). For the PDHIGHCOMB scenario we applied a global factor of 5 increase to PIBASE anthropogenic combustion emissions, in line with recent observations of their potential magnitude (Conway et al., 2019; Matsui et al., 2018). In the FU we assumed that anthropogenic emissions will follow the intermediate emissions scenario “RCP4.5” pathway, and a monthly PD:FU fossil fuel BC emission ratio (Figure S2) was applied to PD anthropogenic combustion iron emissions to estimate their FU flux. Based on the global mean ratio of FU:PD marine BC, we estimated that iron shipping emissions would increase by 65% for the year 2100 respective to PD levels.

### 2.3. Soluble Iron Module

Using an intermediate-complexity soluble iron mechanism, suitable for use within a global Earth system model (Scanza et al., 2018), three major sources of soluble iron were examined in this study: mineral dust, fires, and anthropogenic combustion (sum of industrial, domestic, and shipping combustion). A detailed description of the atmospheric processing of aerosol iron within the model was reported by Scanza et al. (2018). Briefly, both a proton- and an organic ligand-promoted iron dissolution mechanism are included in this study. The proton-promoted dissolution scheme depends upon temperature and an assumed  $[\text{H}^+]$ , based on the simulated mass mixing ratio of sulfate:calcite in each model grid cell. The organic ligand dissolution scheme depends upon the organic carbon concentration, which is used as a proxy for oxalate concentrations. Comparisons of the model's iron dissolution mechanisms used here with observations and other models have been conducted by Scanza et al. (2018) and Hamilton et al. (2019).

The solubility of PD and FU anthropogenic combustion iron was set global at 4% (Luo et al., 2008). In the absence of PI domestic wood burning iron solubility measurements, we have assumed that a 10% iron solubility, based on the lower and upper limits of PD coal iron solubility (Chen et al., 2012, at 20% and Desboeufs et al., 2005, at 0.2%), is representative for PI domestic wood fuel combustion. However, as PI domestic fuels are negligible in terms of the mass of soluble iron emissions, our assumption of a higher solubility for this fuel source does not impact our results. The soluble fraction of iron in bunker fuels used in shipping is uncertain and ranges from 36–79% in the literature (Oakes et al., 2012; Schroth et al., 2009). Here we used a lower limit of 36% in the PDBASE case and an upper limit of 79% for the PDHIGHCOMB and FUBASE cases. At emission, the fine mode iron aerosol from fires solubility was set to 33%, between literature estimates of 12–46% (Ito, 2013; Oakes et al., 2012), and in coarse mode was lower at 4% as used by Luo et al. (2008). In setting global solubility values we did not account for regional differences in the composition of fuel types or any differences in technology employed in its combustion. For example, iron solubility can be affected by either the temperature at which the fuel is combusted altering the mineralogical composition (Journet et al., 2008; Mitchell & Gluskoter, 1976) or due to differential sulfate association (Fu et al., 2012; Oakes et al., 2012; Schroth et al., 2009).

### 2.4. Ocean Biogeochemical Model

We examined how changing the atmospheric flux of soluble iron impacts marine biogeochemistry with the ocean component of the CESM. Here we used a modified version of CESM 1.21 that includes many of the recent science developments included within CESM v2. This coarse-resolution ( $2\text{--}3^\circ$ ) version of the model has been used recently in a detailed study of the marine nitrogen cycle, including links to the iron cycle (Wang et al., 2019). There are still large uncertainties surrounding the magnitude of different iron sources to the oceans and the losses due to scavenging by sinking particles (Tagliabue et al., 2016). The additional iron sources in our simulations include dissolved iron inputs from sediments ( $20 \text{ Gmol a}^{-1}$ ), hydrothermal vents ( $5.0 \text{ Gmol a}^{-1}$ ), and rivers ( $0.33 \text{ Gmol a}^{-1}$ ). The model includes one explicit iron-binding ligand class with sources due to remineralization and dissolved organic matter production. We do not include any ligand sources from hydrothermal vents or from atmospheric deposition.

The ecosystem includes three explicit phytoplankton functional groups (diazotrophs, diatoms, and smaller phytoplankton), multiple key limiting nutrients (N, P, Fe, and Si), sinking particulates, and both refractory and semilabile dissolved organic matter pools (Moore et al., 2004, Moore, Lindsay, et al., 2013). The Fe:C ratio of the phytoplankton groups varies dynamically in the model as a function of

ambient dissolved iron concentration, ranging between prescribed maximum and minimum values (Moore et al., 2004). In this study, we allowed for a wider range of Fe:C ratios (or iron quotas) by the phytoplankton than in most biogeochemical models and prior studies with this model (previously the range was from 3.0 to 6.0  $\mu\text{mol Fe mol}^{-1}$  C; Moore et al., 2004, 2006; here it ranges from 3.0 to 30  $\mu\text{mol Fe mol}^{-1}$  C). This range is in better agreement with the limited in situ observations of phytoplankton iron quotas, mainly from HNLC regions, where observed Fe:C ratios are often in the range of 10 to 30  $\mu\text{mol Fe mol}^{-1}$  C (King et al., 2012; Twining et al., 2011). This wider range gives plankton more capacity to acclimate to ambient dissolved iron concentrations, reducing their uptake when iron is scarce, and increasing iron uptake in high-iron areas associated with major dust plumes and the continental margins. This has the effect of damping the ocean biogeochemical response to variations in atmospheric soluble iron deposition.

The experiments were designed to examine the longer-term responses (multicentury) to changing the atmospheric soluble iron deposition flux. Iron scavenging parameters were optimized using the PDBASE atmospheric iron deposition flux (current era deposition, concurrent with the in situ iron observations used to evaluate the atmosphere model). The model was then spun up for 500 years with the PIBASE soluble iron deposition flux. Six branch simulations forced by our six iron deposition estimates were then extended for an additional 300 years. Here, we analyze annual model output averaged over the last 20 years of these 300-year simulations. Three hundred years is sufficient for upper ocean biogeochemistry to fully adapt to the change in iron inputs from the atmosphere. The branch simulations included a dynamic, single-box, atmospheric  $\text{CO}_2$ , that is a function of only the simulated air-sea  $\text{CO}_2$  flux. We reported the integrated changes in atmospheric  $\text{CO}_2$  concentration over the full 300-year simulation.

### 3. Results and Discussion

#### 3.1. Past, Present, and Future Iron Emissions

There are large uncertainties in the reconstruction of dust in different regions over the historical time period (e.g., Ginoux et al., 2004; Mahowald et al., 2010; Yoshioka et al., 2005). In this study, PI dust emissions are estimated to be approximately two thirds (63%) PD levels (from 1,775 to 1,112  $\text{Tg a}^{-1}$ ; Table 2), as discussed in more detail in section 2.

The amount of carbon emitted and the area burned in fires decreases between the PI and PD (Hamilton et al., 2018), while anthropogenic combustion emissions increase (Dentener et al., 2006; Lamarque et al., 2010). Across the following uncertainties in pyrogenic emissions, we find that pyrogenic iron emissions in the PI were likely within the range of 1.5 to 2.8  $\text{Tg a}^{-1}$ , and in the PD are likely within the range of 1.6 to 3.4  $\text{Tg a}^{-1}$ . In the PIHIGHCOMB emission scenario anthropogenic combustion iron emissions were increased from <1% to 20% of PD levels, based on Scanza et al. (2018) which assumed they scale with CMIP5 estimates of historical industrial BC emissions (Lamarque et al., 2010), resulting in anthropogenic combustion iron emissions increasing from  $0.70 \times 10^{-3}$  to 0.13  $\text{Tg a}^{-1}$ . Fire emissions were also increased for PIHIGHCOMB by replacing SIMFIRE-BLAZE estimates with those from the LMfire model (Hamilton et al., 2018; Pfeiffer et al., 2013), resulting in PI fire iron emissions increasing from 1.5 to 2.7  $\text{Tg a}^{-1}$ . The approximate factor of 2 increase in PI fire emissions between the two fire models is due in part to different representations of how anthropogenic land use and land cover change over the historical period affect burnt area, and thus emission, as well as LMfire containing an additional emission source from agricultural fires. In the PDHIGHCOMB emission scenario the model simulations are brought into better agreement with recent iron observations (Conway et al., 2019; Matsui et al., 2018) by applying a global uniform factor of 5 multiplier to the Luo et al. (2008) anthropogenic combustion iron emissions used in the PDBASE simulation, resulting in anthropogenic combustion iron emissions increasing from 0.68 to 3.4  $\text{Tg a}^{-1}$ . Over the Industrial Era, reductions to fire iron emissions may be partially offsetting increases in dust iron emissions, but likely restricted to the Southern Hemisphere (SH) where the dust loadings and anthropogenic combustion emission increases are both smaller than in the Northern Hemisphere (NH).

Over the current century we predict that the downward trend in fire iron emissions reverses as PD to FU fires increase (Ward et al., 2012), while anthropogenic emissions are, globally, predicted to decrease (Tables 1 and 2 and Figure S2). Future changes in fires are highly uncertain, depending on projections of how climate change, population growth, and increased atmospheric  $\text{CO}_2$  impact burnt area (Knorr et al., 2016). The net

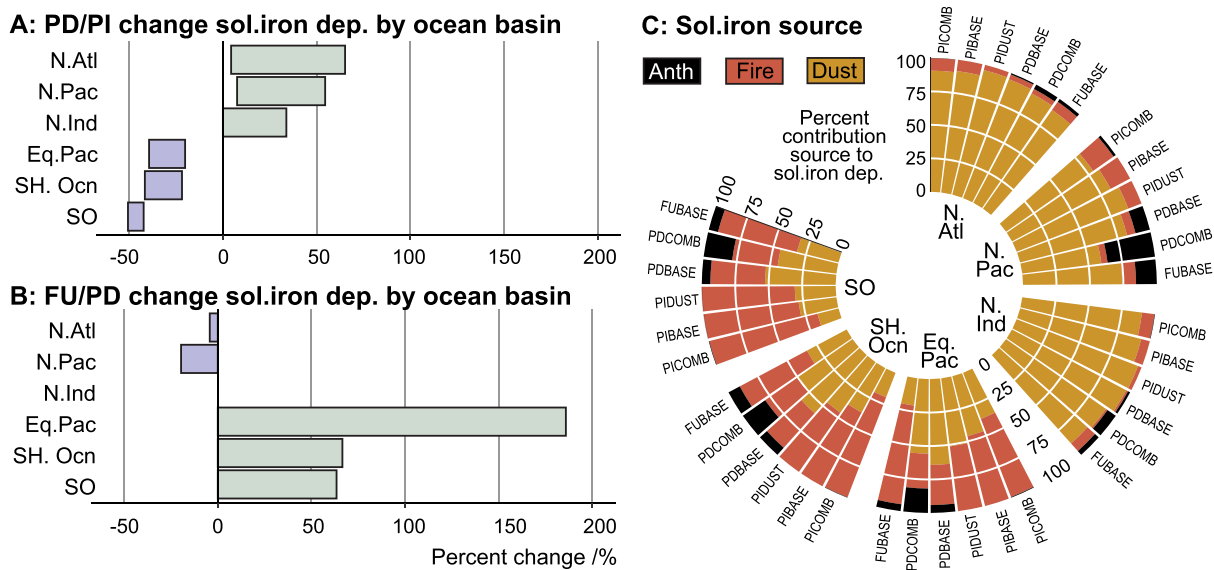


**Figure 1.** Change in soluble iron deposition from preindustrial to present day (a; PD/PI) and from present day to future (b; FU/PD). Time periods are PI (ca. 1750 CE), PD (ca. 2008 CE), and FU (ca. 2100 CE). Soluble iron deposition source shown for each case (c); PICOMB: PIBASE with increased fire and anthropogenic combustion emissions; PIBASE: PI base scenario; PIDUST: PIBASE with PD dust; PDBASE: PD base scenario; PDCOMB: PD with increased (x5) anthropogenic combustion emissions; FUBASE: 2100 emissions following RCP4.5, note that the FU/PD change has PDCOMB as the baseline (Table 1), and the change would thus be higher if PDBASE were instead used. Ocean basins are North Atlantic (N.Atl), North Pacific (N.Pac), North Indian (N.Ind), Equatorial Pacific (Eq. Pac), Southern Atlantic, Pacific and Indian (SH. Ocn), and the Southern Ocean (SO).

effect on fire emissions will depend on what type of vegetation is being combusted on the area burnt. The RCP4.5 scenario results in a global one-third decrease in anthropogenic BC combustion emissions by 2100, although some regions (mainly Africa and South East Asia) do increase (Figure S2), resulting in predicted soluble iron emissions from anthropogenic combustion decreasing from 3.4 to 2.4 Tg  $\text{a}^{-1}$ . End of the century increases to Arctic and SH shipping transport routes are not accounted for as FU shipping emissions are estimated by applying a uniform ratio (1.65) to PD shipping emissions, and thus FU emissions have the same spatial distribution as the PD.

### 3.2. Past, Present, and Future Oceanic Soluble Iron Deposition

To understand the extent to which anthropogenic activity alters the magnitude of soluble iron deposition to the oceans, we compare the PI to PD (Figure 1a) and PD to FU (Figure 1b) flux in six ocean basin regions from paired (base and perturbed) scenarios. Meteorology is fixed in all time periods, and thus changes in deposition flux are due only to simulated changes in emissions and not transport pathways. From PI to PD there is a clear northward gradient in the atmospheric deposition flux of soluble iron to the oceans. Over the Industrial Era, we estimate that NH ocean basin soluble iron deposition has increased (PD/PI percent change: North Atlantic = 4% to 64%, North Pacific = 8% to 55%, North Indian = 0% to 32%), while SH ocean basin deposition has decreased (PD/PI percent change: equatorial Pacific = -20% to -39%, Southern [Atlantic + Pacific + Indian] = -22% to -42%, Southern Ocean = -42% to -50%). In contrast, from the PD to FU this gradient reverses following RCP4.5 with the strongest 21st Century change occurring within the SH (FU/PD percent change: equatorial Pacific = 186% to 229%, Southern [Atlantic + Pacific + Indian] = 67% to 92%, Southern Ocean = 63% to 95%). Overall, the predicted PI to PD increase in ocean deposition for this study ranges from 1.0% to 65%. Other modeling studies (Ito & Shi, 2016; Luo et al., 2008; Myriokefalitakis et al., 2015) have previously reported that since the PI human activity may have increased the atmospheric soluble iron flux to the oceans by between 80% and 200% (Ito & Shi, 2016 and references within). However, by not fully accounting for how anthropogenic activity and land use/cover change alters iron emissions, previous studies yielded a PI soluble iron atmospheric burden which is lower than presented here (Table S2).

The relative contribution of each iron source in different basins varies at each studied emissions time period (Figure 1c). For the three sensitivity experiments, soluble iron emissions were increased for three sources:

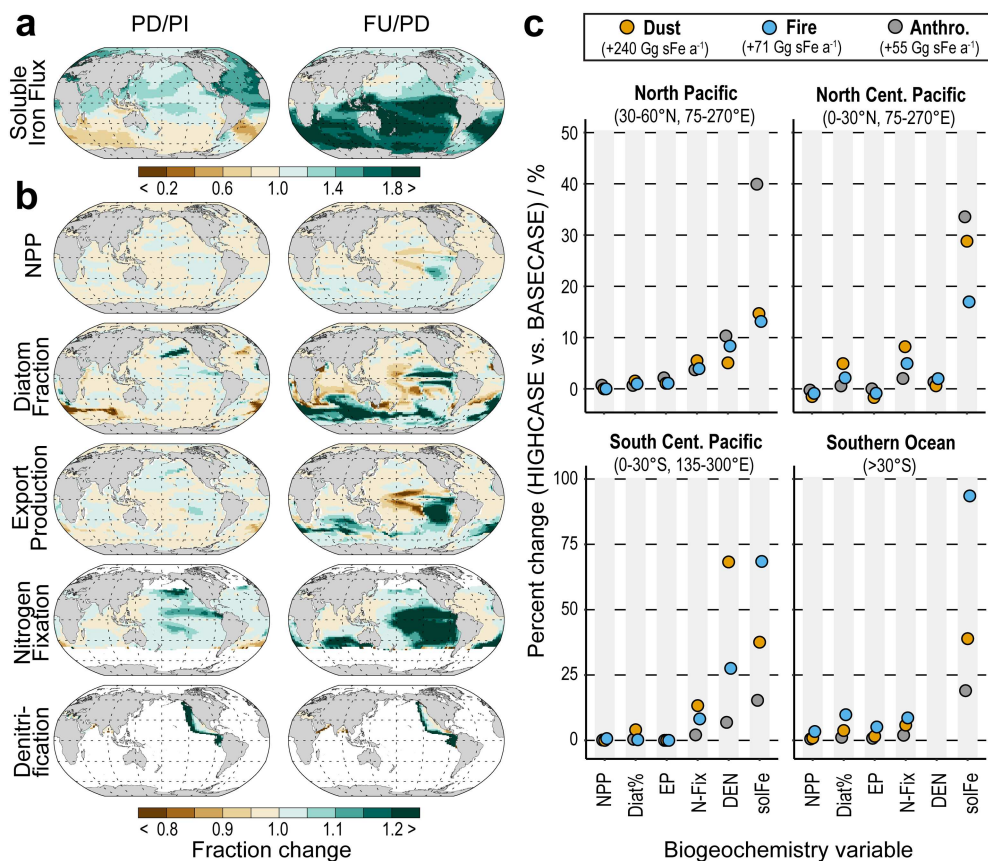


**Figure 2.** Change in atmospheric deposition of soluble iron (a) and ocean biogeochemistry response (b, c) in net primary productivity (NPP), fraction of NPP from diatoms (Diat%), export production (EP), Nitrogen Fixation (N-Fix), and denitrification (DEN). Panel b shows response due to panel a; panel c shows response due to emission uncertainty in each source. Additional soluble iron (solFe) ocean flux due to emission uncertainty in PI dust and fires and PD anthropogenic combustion shown in legend (c).

PD anthropogenic combustion, PI fire, and PI dust emissions, increasing the atmospheric deposition flux to the oceans by 55, 71, and 240 Gg a<sup>-1</sup>, respectively, compared to their paired base case. Within the NH, PI to PD increases in soluble iron deposition are driven by the 60% increase in dust loading, in response to historical land use and land cover changes, and the new source of iron from anthropogenic combustion activity; however, predicted policy controls over the 21st century reduces the relative importance of anthropogenic combustion (~70% decrease in iron from NH anthropogenic combustion sources by 2100), particularly from Asia as seen in the Northern Pacific deposition reduction. Predicted end of the century increases in fires balance industrial emission controls, resulting in little overall change to the net soluble iron deposition from PD to FU across the NH. Dust emissions tend to increase with rising temperature (Kok et al., 2018) and in some regions are becoming more frequent and intense (Namdari et al., 2018); however, the methodology adopted here results in a small (4%) decrease in soluble iron deposition from dust being predicted for 2100.

The drivers for past changes in fires are different from future ones; PI to PD reductions in global burnt area (Arora & Melton, 2018; Hamilton et al., 2018; Mallek et al., 2013) are primarily driven by increasing human population density and changing land management practices (Andela et al., 2017; Bistinas et al., 2013; Hantson et al., 2015; Knorr et al., 2014), while future increases in burnt area (Ward et al., 2012) are more likely to be the result of a warmer, drier climate (Pechony & Shindell, 2010). Future fire emission increases used here are primarily due to changes in the length and intensity of the dry season combined with enhanced gross primary production increasing the fuel load in a warmer climate, with changes due to direct human activity increasing ignitions and altering land use being a secondary effect (Kloster et al., 2012a,

2012b; Ward et al., 2012). Shifting the pyrogenic iron source from industry to fires therefore removes a large degree of human control over these emissions as well as increasing the interannual variability in their magnitude. The SH ocean iron flux is more sensitive to assumptions in how fires evolve in response to human activity and climate change than the NH where dust and anthropogenic sources of soluble iron are dominant (Ito et al., 2019; Ito & Shi, 2016; Matsui et al., 2018). Modeling studies suggest that in a future warmer, wetter climate, fires will increase across the extratropics and decrease across the tropics (Kloster et al., 2012b; Veira et al., 2016). A future poleward migration of fire distribution is important when we consider that dust sources are generally closer to the equator; therefore, regions where fire has a major contribution to soluble iron deposition are found within higher latitudes away from this source (Hamilton et al., 2019).

The rate of iron dissolution into its soluble form is sensitive to the aerosol pH (Meskhidze et al., 2003; Solmon et al., 2009) and hence assumptions about the concentration of acidic compounds present in the atmosphere. Here we parameterize aerosol pH in each grid cell to depend on the ratio of sulfate to calcite, the dominant species governing pH at that time and location (Scanza et al., 2018). Although relatively basic in concept, model results suggest our pH parametrization captures much of the distribution that a more complex aerosol pH scheme would and is computationally efficient; therefore, this parametrization is reasonable for use in an Earth System Model (Hamilton et al., 2019). In the absence of significant industrial activity in the PI, fire SO<sub>2</sub> becomes a relatively more important source of acidity compared to the PD. The approximate doubling of SO<sub>2</sub> fire emissions from LMFIRE compared to SIMFIRE-BLAZE simulations resulted in an additional 7% deposition in dust soluble iron between PIBASE and PIHIGHCOMB simulations. Despite large reductions in SO<sub>2</sub> imposed by air quality acts (Turnock et al., 2015) PD aerosol still exhibits high acidity (Weber et al., 2016), which will help retain present levels of iron acid processing if it persists in the future.

### 3.3. Anthropogenic Iron Impact on Ocean Biogeochemistry

Phytoplankton require iron for photosynthesis, respiration, and nitrogen fixation (Tagliabue et al., 2017). When iron is the limiting nutrient for phytoplankton growth in some regions (e.g., HNLC ocean regions) its addition has been shown to increase phytoplankton biomass and productivity (Boyd et al., 2007; de Baar et al., 2005). The six ocean biogeochemistry simulations in this study varied the magnitude of the global atmospheric soluble iron deposition flux from 0.46 to 0.77 Tg a<sup>-1</sup>. Contrary to previous studies with this model (Krishnamurthy et al., 2009; Mahowald, Lindsay, et al., 2011), but consistent with other studies (Bopp et al., 2013; Wang et al., 2015), we find that global total ocean net primary production (NPP) is insensitive to these changes in atmospheric soluble iron deposition. Nitrogen fixation, denitrification, phytoplankton community structure, and particulate carbon export alter more across large regional scales in response to changing soluble iron flux (Figure 2 and Table S3). The global carbon export efficiency for pyrogenic and lithogenic iron sources (between ~210 and ~1,900 g of carbon sequestered per gram of dissolved iron added) is within the range of low (from -15 to 1.0) and high (from 2,500 to 14,000) sensitivity models (Ito et al., 2020). To our knowledge, the CESM (this study), RECoM2 (Ye & Völker, 2017), MIROC-ES2L (Hajima et al., 2019; Watanabe et al., 2018), and NEMO-PISCES (Aumont et al., 2015; Wang et al., 2015) ocean models currently contain options for including a pyrogenic iron ocean input, which will be further examined in the framework of the iron model intercomparison project (FeMIP) (Tagliabue et al., 2016).

The PIHIGHDUST and PIHIGHCOMB sensitivity experiments examined how the large uncertainty in PI aerosol emission sources altered the magnitude of the oceanic soluble iron deposition flux. Similar to the results of in situ ocean iron fertilization experiments (Boyd et al., 2007; Moore, Mills, et al., 2013), the biogeochemistry of the eastern Pacific and Southern Ocean are most sensitive to changes in the soluble iron flux (Figure 2). By source, the largest uncertainty in oceanic soluble iron deposition comes from the representation of PI dust emissions (PIHIGHDUST deposits 240 Gg soluble Fe a<sup>-1</sup> more to the oceans than PIBASE). Due to offsetting regions of increasing and decreasing NPP, increasing iron deposition from dust sources results in a global NPP change close to 0 (PIHIGHDUST compared to PIBASE). Increasing PI pyrogenic emissions results in a change in soluble iron deposition which is ~70% lower than that for the PIHIGHDUST case (PIHIGHCOMB deposits 71 Gg soluble Fe a<sup>-1</sup> more to the oceans than PIBASE) but increases global NPP by 0.7% (PIHIGHCOMB compared to PIBASE). Compared to dust, uncertainty in

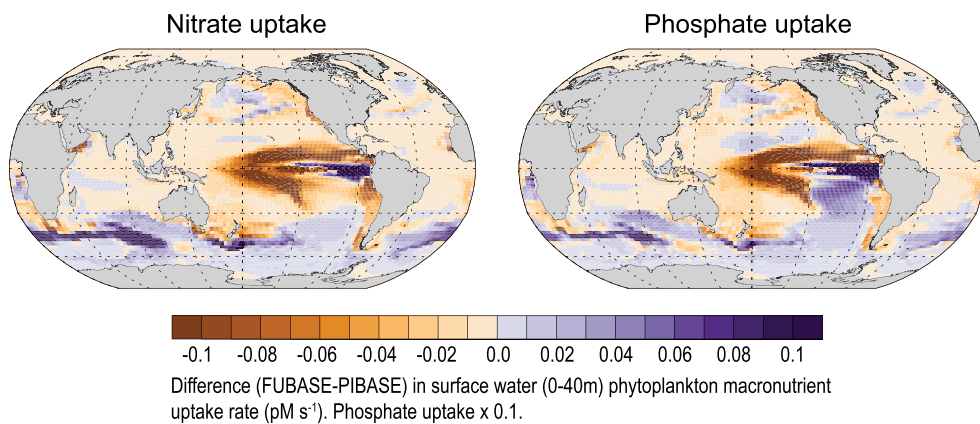


**Figure 3.** Difference in surface (0–40 m) macronutrient uptake rate by all phytoplankton groups (sum of diatoms, diazotrophs, and small phytoplankton) between the FUBASE and PIBASE simulations. Shown for top 40 m as NPP response to increasing atmospheric soluble iron deposition is opposite below this level (Figure 5).

pyrogenic sources of iron therefore has a disproportionate impact on NPP as fire emissions favor deposition to iron-limited regions more than dust sources (Figure 2c).

In the equatorial Pacific, upwelling brings macronutrients to the surface waters. Iron limitation restricts macronutrient uptake by phytoplankton, resulting in the lateral spread of surplus macronutrients away from upwelling zones. Figure 3 shows that along the equatorial Pacific upwelling region, reductions in the iron deficit, from an increased atmospheric soluble iron flux, increases macronutrient uptake by phytoplankton and thus NPP increases (Figure 2). However, the increased rate of macronutrient uptake reverses away from the upwelling zone, decreasing NPP and altering the boundary between the iron-limited HNLC region and the surrounding nitrogen-limited waters (Figures 4 and S3). This pattern of increased (decreased) macronutrient uptake and NPP in one area being at least partially offset by decreased (increased)

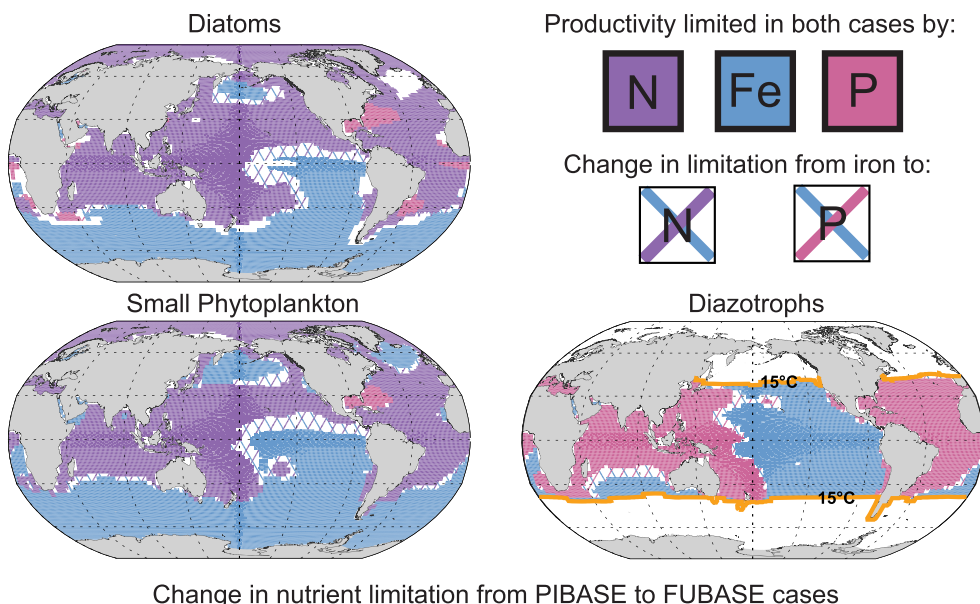


**Figure 4.** Location of phytoplankton nutrient limitation shift from iron to nitrogen (e.g., diatoms and small phytoplankton) or phosphorus (e.g., diazotrophs) due to an increased soluble iron flux from the atmosphere. Change to silica limitation omitted for diatoms (white space). Diazotrophs are not present in the model at high latitudes where temperatures are below  $\sim 15^{\circ}\text{C}$ . Shown for change from PIBASE to FUBASE cases (Table 1), comparisons with increasing fire and dust iron sources shown in Figure S3.

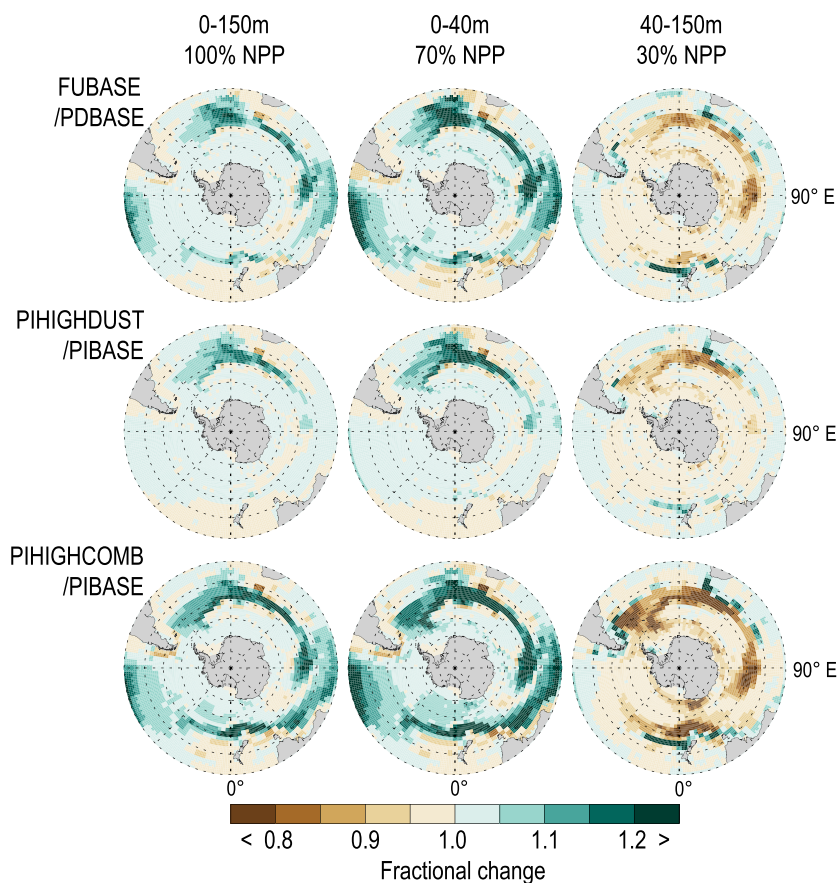


**Figure 5.** Net primary productivity changes due to increases in the atmospheric soluble iron flux. Majority (70%) of NPP within euphotic zone (0–150 m) is in the top 40 m. Below this level the response to soluble iron addition is opposite to above it.

macronutrient uptake and NPP in “downstream” waters, particularly in the equatorial Pacific region, is common in all our simulations and partially explains the small overall impacts of increasing soluble iron deposition on global-scale NPP (Table S3).

In addition to horizontal shifts in ocean productivity, there is a change in the vertical distribution of ocean productivity (Figure 5). The majority (70%) of global NPP occurs within the top 40 m. However, below 40 m the response of NPP to soluble iron addition is opposite to that above it. Reductions in iron nutrient stress favors the growth of the larger diatom phytoplankton species, which are more efficient (by a factor of ~3 in this model version) in exporting carbon to the interior ocean (Fu et al., 2016). Stimulation of phytoplankton growth by increasing deposition will increase biomass (and chlorophyll) concentrations in the upper ocean, often attenuating the light flux to the lower euphotic zone—hibiting deep productivity. Conversely, increasing iron stress will decrease growth rates and biomass, amplifying the light flux to the deeper euphotic zone—boosting deep productivity. Thus, it is the interplay of both light and nutrient availability driving the contrasting vertical response patterns seen in Figure 5. Shifting productivity upwards in the euphotic zone results in more of the generated sinking organic matter being regenerated within the upper euphotic zone, decreasing the carbon export efficiency below a fixed depth (often over 100 m) and likely tempering the overall carbon export gains due to an increased soluble iron deposition flux.

Figure 2 shows that while perturbations to the carbon cycle are most sensitive within the SH oceans below 30°S (particularly within the Southern Indian Ocean), changes to the nitrogen cycle are most sensitive within the south central Pacific (0–30°S) region (Figure 2c) which is thought to be more iron-limited than other subtropical gyres (Martiny et al., 2019). Furthermore, nitrogen fixation by diazotrophs, which are thought to have a higher iron requirement (Capone et al., 1997; Hutchins & Boyd, 2016), and

denitrification are both more sensitive to changes in the magnitude of soluble iron deposition than NPP and carbon export (Figure 2). Globally, there has been an approximately 2% increase in the modeled amount of fixation from PI to PD. By source we find that changes in pyrogenic iron emissions introduces a 3% to 8% decrease in nitrogen fixation over the Industrial Era, which is offset by at most a 6% increase from increasing dust emissions. Changes to denitrification are globally the most sensitive parameter investigated (Figure 2). Globally, decreasing PI to PD fire iron emissions reduces denitrification by between 8% and 15%, offset by increasing industrial and dust emissions increasing denitrification by 13% and 3%, respectively.

Under RCP4.5, our estimate of iron emission increases from PD to FU are smaller than from PI to PD (Table 2); however, the SH response in ocean biogeochemistry is predicted to be much larger (Figure 2b). This is due to the competing effect of increases to dust-source iron and decreases to fire-source iron from PI to PD not continuing into the future. Instead, fires increase substantially to reach near equivalence with anthropogenic combustion emission levels (2.3 and 2.4 Tg Fe  $a^{-1}$  at 2100 for fires and anthropogenic sources, respectively). Future consolidation of pyrogenic iron sources, which exhibit a high iron solubility (Ito et al., 2019), within the SH results in potentially large impacts for the future of the carbon and nitrogen cycles which are sensitive to changes in iron deposition flux in this half of the globe. We predict that nitrogen fixation increases by ~9% globally (up to a maximum of 24% in the south central Pacific: 0–30°S, 135–300°E) by the end of the century, due to the increased iron supply easing previous diazotroph iron limitation, particularly within the eastern Pacific.

### 3.4. Regional Ocean Responses to Altering Atmospheric Soluble Iron Flux

Across our estimated range in PI to PD and PD to FU changes to atmospheric soluble iron deposition to the oceans, Figure 2 shows how reducing phytoplankton iron limitation in the upwelling region of the equatorial Pacific stimulates productivity near the equator. Increasing productivity at the equator requires an increased phytoplankton macronutrient consumption rate, concurrently reducing the macronutrient consumption rate downstream, as upwelled waters spread laterally (Figure 3). Increasing the atmospheric soluble iron flux also modifies the spatial distribution of nutrient limitation, reducing the extent of iron limitation in the Pacific (Figures 4 and S3). This spatial shifting of the rate of macronutrient consumption by phytoplankton, in response to an increased iron flux, results in a compensating effect on NPP at the basin scale. In contrast, the Southern Ocean remains iron-limited throughout our simulations (e.g., Figure 4), with excess nutrients subducting within Antarctic Intermediate and Subantarctic Mode waters, and thus become unavailable within the euphotic zone. Compared to the equatorial Pacific region, the macronutrient uptake rate by phytoplankton within lower latitudes increases with increasing soluble iron deposition; therefore, the response of NPP across the Southern Ocean to atmospheric soluble iron deposition is more unidirectional (Figure 2).

A community shift from dominance by small phytoplankton toward increasing diatom dominance has been observed in in situ iron fertilization experiments (Boyd et al., 2007; de Baar et al., 2005; Fu et al., 2016). Our results are thus consistent with the idea that an increased soluble iron deposition flux (e.g., Last Glacial Maximum) could result in a greater proportion of the phytoplankton community shifting from smaller phytoplankton to larger diatoms than presented here in Figure 2, and hence increase global air-sea CO<sub>2</sub> exchange further (Kohfeld & Ridgwell, 2009). Over much of the Southern Ocean smaller phytoplankton dominate the phytoplankton community, but in areas where additional iron is available phytoplankton blooms are dominated by the larger sized diatoms, which are more efficient in exporting carbon to the ocean interior (Fu et al., 2016). Thus, the response of Southern Ocean biogeochemistry to variations in atmospheric iron inputs is strongly dependent on the phytoplankton community structure.

### 3.5. Improvements to and Contrasts With Previous Studies

Iron is an essential nutrient for supporting the growth of marine organisms (Tagliabue et al., 2017). Yet our ocean biogeochemistry model results suggest that when climate forcings and other marine sources of iron are held constant, global NPP is largely insensitive to anthropogenically mediated changes to the magnitude of the atmospheric soluble iron flux, even across a large range of Anthropocene soluble iron emissions and deposition scenarios (Figure 6). This result suggests that the current version of this ocean model has a lower sensitivity to iron deposition than previous versions (e.g., Krishnamurthy et al., 2009; Mahowald, Ward, et al., 2011, 2010). Modeled marine responses to changing soluble iron inputs are likely sensitive to the

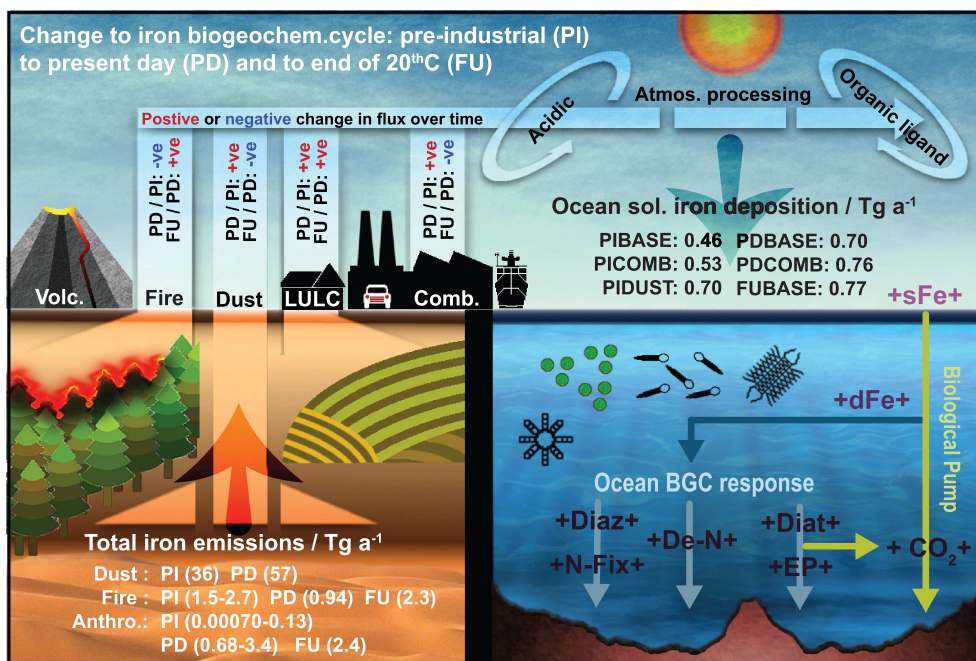


**Figure 6.** Iron biogeochemical cycle schematic. Range (base to high) of iron emissions ( $\text{Tg Fe a}^{-1}$ ) for preindustrial (PI; ca. 1750 CE), present day (PD; ca. 2008 CE), and the future (FU; ca. 2100 CE) shown (Table 1). Deposition of soluble iron ( $\text{Tg Fe a}^{-1}$ ) to global oceans from the six simulations investigated in this study also shown (Figure 1). Simulations: PI dust and fires with no industry (PIBASE); PI dust with higher PI fires and 20% PD industry (PICOMB); PD dust, PI fires, and no industry (PIDUST); PD dust, fires, and industry (PDBASE); PD dust, fire, and  $\times 5$  industry (PDCOMB); FU dust, fire, and industry (FUBASE). LULC = anthropogenic land use land cover change. Volcanic emission source assumed to not change with time or human activity and is shown for completeness only.

details of both the atmospheric soluble iron deposition and the ocean biogeochemical model. However, the overall quantitative results (e.g., the importance of a wildfire iron source for the Southern Ocean) are likely to be robust across models, as the underlying spatial distribution of soluble iron from dust and pyrogenic emission sources are still similar.

Early marine biogeochemical models included only the atmospheric source from dust for external iron inputs to the oceans. Over time the addition of iron sources from sediments, hydrothermal vents, riverine sources, and glacial processes have weakened the sensitivity to atmospheric deposition (Tagliabue et al., 2016). One recent study suggested a high sensitivity of global NPP to changes in atmospheric inputs, but is relatively insensitive to varying sedimentary source strengths (Ito et al., 2020). However, the details of how the particle-scavenging removal of dissolved iron is parameterized varies greatly across current ocean biogeochemical models (Tagliabue et al., 2016). The rate of removal by scavenging determines how far dissolved iron will be advected from its source region before being ultimately lost to ocean sediments. Thus, the relative importance of different iron sources in supporting biological production is strongly dependent on the (highly uncertain) scavenging mechanism employed in various models. Ultimately, new observational constraints from GEOTRACES will narrow the uncertainties concerning the magnitude of iron source strengths and losses due to scavenging.

Several factors contribute to the modest NPP response we show here. Adding additional external iron sources to the ocean biogeochemistry model (improved sedimentary source, riverine inputs, and hydrothermal vent inputs) weakened the impacts of variations in the atmospheric soluble iron supply. Similarly, the wider range of potential phytoplankton Fe:C ratios employed here attenuates the impacts of soluble iron deposition on the carbon cycle as phytoplankton biomass and productivity are less sensitive to changing soluble iron inputs. Changing phytoplankton community structure also plays a role, because increasing iron stress can shift the community from diatom-dominated to small phytoplankton-dominated systems. As small phytoplankton export organic matter less efficiently than diatoms, this shift leads to more nutrient

recycling within surface waters and more NPP based on regenerated nutrients. Whereas increasing iron inputs drive the community toward diatom dominance, export becomes more efficient, and less NPP is fuelled by regenerated nutrients. Thus, the varying export efficiency of small and large phytoplankton also acts to attenuate changes in NPP, and may have further implications for higher trophic levels and fisheries (Fu et al., 2016). Lastly, there are often strong, offsetting effects in the oceans “downstream” from regions where soluble iron deposition perturbs biogeochemical cycling, partially attenuating the net effect of additional iron deposition at the basin scale.

Regionally, both PI to PD and PD to FU responses in ocean biogeochemical cycles to changes in soluble iron flux are largest within HNLC regions, as could be expected. The net effect is that despite global NPP remaining constant, regional differences in nitrogen fixation and carbon export result in small changes to atmospheric CO<sub>2</sub> (1–3 ppm), in line with previous model estimates (Krishnamurthy et al., 2009). Overall, we find that nitrogen fixation is most sensitive to perturbations in the atmospheric deposition of soluble iron from dust sources and within the hyperoligotrophic southeast Pacific region. Within the South Pacific (0–30°S) we estimate that future increases in nitrogen fixation are up to an order of magnitude higher than past increases (PD to FU: +24%; PI to PD: +3%). In terms of pyrogenic iron sources, both nitrogen fixation and denitrification are more sensitive to uncertainty in PI fire emissions than the uncertainty in PD anthropogenic combustion emissions, which account for 25% and 43%, respectively, of the change induced by swapping from base (SIMFIRE-BLAZE model) to high (LMfire model) PI fire emissions. Compensating downstream effects on NPP are smallest within the Southern Ocean (>30°S) and we conclude that it is here that deposition changes to soluble iron are most likely to influence net air-sea CO<sub>2</sub> flux and thus climate. In the current climate state atmospheric deposition has significant impacts at midlatitudes, but sedimentary and glacial sources likely dominate the high latitude Southern Ocean (Lancelot et al., 2009; Moore & Braucher, 2008; Tagliabue et al., 2012). Thus, an increased soluble iron deposition flux to the high latitude Southern Ocean at the Last Glacial Maximum does have the potential to significantly alter global nutrient distributions, air-sea CO<sub>2</sub> fluxes, and climate (Marinov et al., 2006; Martin, 1990; Moore et al., 2018).

### 3.6. Future Directions

Improved mechanistic understanding of those parameters controlling the bioavailability of iron, across its atmospheric and oceanic forms, as well as the biotic response, will aid in quantifying the biogeochemical and phytoplankton community response to changes in the atmospheric soluble iron flux. Recent studies (Hamilton et al., 2019; Ito et al., 2019; Mahowald et al., 2018; Meskhidze et al., 2019) all highlight the importance of improving our understanding of iron aerosol properties (e.g., particle morphology, size, and mineralogy), the atmospheric chemistry related to its dissolution (e.g., particle acidity and organic ligand complexation with iron), and loss processes (wet and dry deposition to the ocean) as key areas for future research aimed to reduce uncertainties in our understanding of the atmospheric component of the iron cycle. For dust, improved understanding of the mineralogical distribution of the dust iron emission source environment is important. For example, Hamilton et al. (2019) showed that removing the silt mineral fraction of hematite improved comparisons with the aerosol single-scattering albedo (a critical parameter in estimating the interaction of aerosol with solar radiation) but with an effective reduction of ~30% from coarse-mode hematite (57.5% iron content) emissions. Since wildfires are shown here to be an important source contributing to changes in ocean productivity due to atmospheric deposition of soluble iron within some ocean regions, more constraints on the soluble iron fraction and its dependence on types of wildfires (e.g., forest vs. savannah biomes; e.g., Table 4 in Hamilton et al., 2019) is needed. Furthermore, quantifying the magnitude and composition of crustal material both entrained during a fire and after the biomass is removed is required (Hamilton et al., 2019). Volcanic sources of soluble iron are not included, but may be important (Frogner et al., 2001; Olgun et al., 2011). Improved understanding of the complexity in modeling different atmospheric iron oxidation states could also be important, as well as the inclusion of other metals that may act to modify iron solubility and ocean iron ligand interactions (Meskhidze et al., 2019). Additional laboratory studies defining the properties of iron-bearing aerosol, for example the location and oxidation state of the iron, are important (Meskhidze et al., 2019), as well as the characterization of atmospheric organics which may act as ligands in the ocean as well (Meskhidze et al., 2019).

The impact of an anthropogenic source of other trace metal aerosols important for the ocean carbon and nitrogen cycles was not investigated here. Beyond iron, the atmospheric deposition of copper, zinc,

cadmium, and lead can also impact marine biogeochemistry (Mahowald et al., 2018), and all have a significant anthropogenic component (Pacyna & Pacyna, 2001; Rauch & Pacyna, 2009). In addition to acting as micronutrients, some metals (e.g., copper) can be toxic to phytoplankton at high concentrations (Jordi et al., 2012; Paytan et al., 2009). As the phytoplankton toxicity threshold for copper is tempered by the presence of other metals (e.g., iron and manganese) future studies would need to include a suite of metal aerosols (Mahowald et al., 2018) to diagnose the overall impact. However, copper concentrations may need to be unrealistically high to reduce marine productivity (Zhang et al., 2019).

The residence time of oceanic iron is a potential key uncertainty in linking iron deposition with ocean productivity (Tagliabue et al., 2017). Compared to mineral dust bearing iron particles, smaller sized iron particles from a pyrogenic source may have shorter ocean residence times due to an increased ocean scavenging rate (Tagliabue et al., 2019), which depends on the available metal surface area:volume ratio (Honeyman et al., 1988; Jannasch et al., 1996). Modeling localized aerosol deposition will become important if the dissolved iron residence time is reduced to the order of days (Wingenter et al., 2004), and thus simulations of specific events in models will require greater temporal resolution (Guieu et al., 2014).

Estimating the ocean biotic response to atmospheric iron inputs requires an improved understanding of the response due to other sources of ocean iron, such as sedimentary, riverine, and hydrothermal iron inputs (e.g., Boyd et al., 2017; Hutchins & Boyd, 2016; Tagliabue et al., 2016). However, increasing the complexity of the ocean biotic response to changes in iron bioavailability is a challenge for models as different species may respond differently to the addition of iron as well as other trace metals (Mackey et al., 2015; Mahowald et al., 2018). Furthermore, ocean biota can respond differentially to varying nutrient conditions with flexible stoichiometry (King et al., 2012; Martiny et al., 2013).

Abiotic and biotic sources of ligands, which bind iron and enhance their retention in the ocean, can play an important role in the ocean iron cycle (Boyd et al., 2017; Mahowald et al., 2018; Parekh et al., 2004; Tagliabue et al., 2017). It is possible, but currently poorly understood, that some ocean ligands may be present due to atmospheric deposition (Baker & Croot, 2010; Johnson & Meskhidze, 2013; Meskhidze et al., 2019) and thus are possibly being altered by anthropogenic activity. Variable ligand concentrations could potentially alter the response to fluctuations in atmospheric deposition; however, there are still large uncertainties in the role of ligands in governing iron distributions (Boyd et al., 2017). New observations from the GEOTRACES program are rapidly expanding the observational database for these ligands, leading to new insights into ligand cycling and their interactions with iron (Buck et al., 2015, 2018).

New observations of the coupling between the atmosphere and ocean using novel observational tools including the use of biogeochemical sensors on ARGO floats, ocean gliders, and aircraft could aid in characterizing aerosol properties, impacts on the ocean iron cycle, and the ocean biotic response. In addition, the use of  $^{7}\text{Be}$  water column inventories could aid in furthering our understanding of atmospheric deposition rates (Meskhidze et al., 2019).

#### 4. Conclusions

It is hypothesized that varying the magnitude of the atmospheric soluble iron deposition flux to the oceans has large effects on marine carbon and nitrogen cycles. Our comprehensive study includes an improved representation of iron sources, atmospheric chemistry, and marine biogeochemical cycles; our results demonstrate that changes to the soluble iron deposition flux in the Anthropocene may only have a modest carbon cycle response but a larger impact on the nitrogen cycle. We find that varying the atmospheric soluble iron flux creates strong, offsetting patterns in the marine carbon cycle response. Decreases in phytoplankton macronutrient uptake rates are simulated “downstream” from where an increased soluble iron flux increases uptake rates, partially attenuating the net response of NPP and carbon export to varying the atmospheric soluble iron flux at the basin scale. Such downstream effects will need to be accounted for when determining the appropriate carbon sequestration credits for any proposed iron fertilization of the oceans for climate “geoengineering.”

Anthropogenic activity alters atmospheric soluble iron deposition to oceans by modifying fire and dust aerosol cycles and by generating additional iron sources through increased industrial, domestic, and shipping emissions. Over the Industrial Era, we show that NH ocean basin soluble iron deposition has likely

increased, while SH ocean basin deposition has likely decreased. We predict that the PI to PD shift in the locus of soluble iron deposition reverses by 2100 following RCP4.5, as SH anthropogenic activity and fires become more important due to changes in demographics and climate. In all our simulations here, the equatorial Pacific and Southern Ocean regions are still strongly iron limited. Thus, there is the potential for larger perturbations if atmospheric iron deposition is further increased. As the response of the marine carbon and nitrogen cycles to changes in the soluble iron flux is strongest within SH oceans, we can expect human activity to continue to have an important influence on iron-mediated biogeochemical cycling into the future.

The impact of changes in soluble iron deposition on atmospheric CO<sub>2</sub> concentrations is highly uncertain and cannot be characterized by a single metric. We find, however, that in the Southern Ocean (>30°S), carbon export efficiency (gram of carbon sequestered per gram of soluble iron deposited) is 43% larger when altering PI fire emissions compared to dust emissions (~7,600:1 for fires and ~5,300:1 for dust) with corresponding decreases in CO<sub>2</sub> of 2.8 and 1.3 ppm, respectively. Modeling long-term changes in iron-mediated biogeochemical cycles thus requires information on how both fires and dust have changed in the past and will be sensitive to assumptions in how land use/cover and fires will evolve in the warming climate of the future.

## Data Availability Statement

Data available on the Cornell eCommons repository (<https://doi.org/10.7298/fbd6-sg85>).

## Author Contributions

D. S. H. performed atmospheric simulations, wrote the manuscript with support from J. K. M. and N. M. M., and prepared all figures and tables. J. K. M. performed ocean simulations. A. A., S. H., J. O. K., and L. N. performed fire model simulations. A. I. provided shipping emissions. T. C. B. and S. D. R. provided preindustrial estimates of anthropogenic iron. All authors edited manuscript text.

## Acknowledgments

This work was supported by Department of Energy (DOE) and National Science Foundation (NSF) grants for atmospheric deposition impacts on ocean biogeochemistry (DE-SC0016362, NSF 1049033, and CCF-1522054). D. S. H. was also supported by the Atkinson Center for a Sustainable Future. J. K. M. was also supported by DOE Grant DE-SC0016539. A. A. would like to thank the Helmholtz Foundation, its ATMO program, and its impulse and integration fund. T. C. B. and S. D. R. thank the NSF grant (1049033) for its support. This material is based upon work supported by the National Center for Atmospheric Research, which is a major facility sponsored by the National Science Foundation under Cooperative Agreement 1852977. We would like to acknowledge high-performance computing support from Cheyenne (doi:10.5065/D6RX99HX) provided by NCAR's Computational and Information Systems Laboratory, also sponsored by the National Science Foundation. We are grateful to both referees (Philip Boyd and one anonymous) for their constructive input during peer review.

## References

- Alves, C., Gonçalves, C., Fernandes, A. P., Tarelho, L., & Pio, C. (2011). Fireplace and woodstove fine particle emissions from combustion of western Mediterranean wood types. *Atmospheric Research*, 101(3), 692–700. <https://doi.org/10.1016/j.atmosres.2011.04.015>
- Andela, N., Morton, D. C., Giglio, L., Chen, Y., van der Werf, G. R., Kasibhatla, P. S., et al. (2017). A human-driven decline in global burned area. *Science*, 356(6345), 1356–1362. <https://doi.org/10.1126/science.aal4108>
- Arora, V. K., & Melton, J. R. (2018). Reduction in global area burned and wildfire emissions since 1930s enhances carbon uptake by land. *Nature Communications*, 9(1), 1326. <https://doi.org/10.1038/s41467-018-03838-0>
- Aumont, O., Bopp, L., & Schulz, M. (2008). What does temporal variability in aeolian dust deposition contribute to sea-surface iron and chlorophyll distributions? *Geophysical Research Letters*, 35, L07607. <https://doi.org/10.1029/2007GL031131>
- Aumont, O., Ethé, C., Tagliabue, A., Bopp, L., & Gehlen, M. (2015). PISCES-v2: An ocean biogeochemical model for carbon and ecosystem studies. *Geoscientific Model Development*, 8(8), 2465–2513. <https://doi.org/10.5194/gmd-8-2465-2015>
- Baker, A. R., & Croat, P. L. (2010). Atmospheric and marine controls on aerosol iron solubility in seawater. *Marine Chemistry*, 120(1–4), 4–13. <https://doi.org/10.1016/j.marchem.2008.09.003>
- Bistinas, I., Oom, D., Sá, A. C. L., Harrison, S. P., Prentice, I. C., & Pereira, J. M. C. (2013). Relationships between human population density and burned area at continental and global scales. *PLoS ONE*, 8(12), e81188. <https://doi.org/10.1371/journal.pone.0081188>
- Böke, H., Göktürk, E. H., Caner-Saltık, E. N., & Demirci, Ş. (1999). Effect of airborne particle on SO<sub>2</sub>-calcite reaction. *Applied Surface Science*, 140(1–2), 70–82. [https://doi.org/10.1016/S0169-4332\(98\)00468-1](https://doi.org/10.1016/S0169-4332(98)00468-1)
- Bond, T. C., Bhardwaj, E., Dong, R., Jogani, R., Jung, S., Roden, C., et al. (2007). Historical emissions of black and organic carbon aerosol from energy-related combustion, 1850–2000. *Global Biogeochemical Cycles*, 21, GB2018. <https://doi.org/10.1029/2006GB002840>
- Bopp, L., Resplandy, L., Orr, J. C., Doney, S. C., Dunne, J. P., Gehlen, M., et al. (2013). Multiple stressors of ocean ecosystems in the 21st century: Projections with CMIP5 models. *Biogeosciences*, 10, 6225–6245. <https://doi.org/10.5194/bg-10-6225-2013>
- Bowie, A. R., Lannuzel, D., Remenyi, T. A., Wagener, T., Lam, P. J., Boyd, P. W., et al. (2009). Biogeochemical iron budgets of the Southern Ocean south of Australia: Decoupling of iron and nutrient cycles in the subantarctic zone by the summertime supply. *Global Biogeochemical Cycles*, 23, GB4034. <https://doi.org/10.1029/2009GB003500>
- Boyd, P., Ellwood, M., Tagliabue, A., & Twining, B. (2017). Biotic and abiotic retention, recycling and remineralization of metals in the ocean. *Nature Geoscience*, 10(3), 167–173. <https://doi.org/10.1038/ngeo2876>
- Boyd, P. W., Jickells, T., Law, C. S., Blain, S., Boyle, E. A., Buesseler, K. O., et al. (2007). Mesoscale iron enrichment experiments 1993–2005: Synthesis and future directions. *Science*, 315, 612–618.
- Brown, A. G., Tooth, S., Bullard, J. E., Thomas, D. S. G., Chiverrell, R. C., Plater, A. J., et al. (2017). The geomorphology of the Anthropocene: Emergence, status and implications. *Earth Surface Processes and Landforms*, 42(1), 71–90. <https://doi.org/10.1002/esp.3943>
- Buck, K. N., Sedwick, P. N., Sohst, B., & Carlson, C. A. (2018). Organic complexation of iron in the eastern tropical South Pacific: Results from US GEOTRACES Eastern Pacific Zonal Transect (GEOTRACES cruise GP16). *Marine Chemistry*, 201, 229–241. <https://doi.org/10.1016/j.marchem.2017.11.007>
- Buck, K. N., Sohst, B., & Sedwick, P. N. (2015). The organic complexation of dissolved iron along the U.S. GEOTRACES (GA03) North Atlantic Section. *Deep-Sea Research Part II: Topical Studies in Oceanography*, 116, 152–165. <https://doi.org/10.1016/j.dsrr.2014.11.016>

- Capone, D., Zehr, J., Paerl, H., Bergman, B., & Carpenter, E. (1997). *Trichodesmium*, a globally significant marine cyanobacterium. *Science*, 276, 1221–1229.
- Chen, H., Laskin, A., Baltrusaitis, J., Gorski, C. A., Scherer, M. M., & Grassian, V. H. (2012). Coal fly ash as a source of iron in atmospheric dust. *Environmental Science & Technology*, 46(4), 2112–2120. <https://doi.org/10.1021/es204102f>
- Chen, Y., & Siefert, R. L. (2003). Determination of various types of labile atmospheric iron over remote oceans. *Journal of Geophysical Research*, 108(24), D4774. <https://doi.org/10.1029/2003JD003515>
- Chuang, P. Y., Duvall, R. M., Shafer, M. M., & Schauer, J. J. (2005). The origin of water soluble particulate iron in the Asian atmospheric outflow. *Geophysical Research Letters*, 32, L07813. <https://doi.org/10.1029/2004GL021946>
- Conway, T. M., Hamilton, D. S., Shelley, R. U., Aguilar-Islas, A. M., Landing, W. M., Mahowald, N. M., & John, S. G. (2019). Tracing and constraining anthropogenic aerosol iron fluxes to the North Atlantic Ocean using iron isotopes. *Nature Communications*, 10(1), 2628. <https://doi.org/10.1038/s41467-019-10457-w>
- de Baar, H. J. W., Boyd, P. W., Coale, K. H., Landry, M. R., Tsuda, A., Assmy, P., et al. (2005). Synthesis of iron fertilization experiments: From the iron age in the age of enlightenment. *Journal of Geophysical Research*, 110, C09S16. <https://doi.org/10.1029/2004JC002601>
- Desboeufs, K. V., Sofikitis, A., Losno, R., Colin, J. L., & Ausset, P. (2005). Dissolution and solubility of trace metals from natural and anthropogenic aerosol/particulate matter. *Chemosphere*, 58(2), 195–203. <https://doi.org/10.1016/j.chemosphere.2004.02.025>
- Dentener, F., Kinne, S., Bond, T., Boucher, O., Cofala, J., Generoso, S., et al. (2006). Emissions of primary aerosol and precursor gases in the years 2000 and 1750 prescribed data-sets for AeroCom. *Atmospheric Chemistry and Physics*, 6, 4321–4344.
- Ellis, E. C., Goldewijk, K. K., Siebert, S., Lightman, D., & Ramankutty, N. (2010). Anthropogenic transformation of the biomes, 1700 to 2000. *Global Ecology and Biogeography*, 19(5), 589–606. <https://doi.org/10.1111/j.1466-8238.2010.00540.x>
- Ellis, E. C., Kaplan, J. O., Fuller, D. Q., Vavrus, S., Klein Goldewijk, K., & Verburg, P. H. (2013). Used planet: A global history. *Proceedings of the National Academy of Sciences of the United States of America*, 110(20), 7978–7985. <https://doi.org/10.1073/pnas.1217241110>
- Falkowski, P. G. (1997). Evolution of the nitrogen cycle and its influence on the biological sequestration of CO<sub>2</sub> in the ocean. *Nature*, 387(May), 272–275.
- Fernandes, S. D., Trautmann, N. M., Streets, D. G., Roden, C. A., & Bond, T. C. (2007). Global biofuel use, 1850–2000. *Global Biogeochemical Cycles*, 21, GB2019. <https://doi.org/10.1029/2006GB002836>
- Frogner, P., Reynir Gislason, S., & Óskarsson, N. (2001). Fertilizing potential of volcanic ash in ocean surface water. *Geology*, 29(6), 487–490. [https://doi.org/10.1130/0091-7613\(2001\)029<0487:FPOVAI>2.0.CO;2](https://doi.org/10.1130/0091-7613(2001)029<0487:FPOVAI>2.0.CO;2)
- Fu, H., Lin, J., Shang, G., Dong, W., Grassian, V. H., Carmichael, G. R., et al. (2012). Solubility of iron from combustion source particles in acidic media linked to iron speciation. *Environmental Science & Technology*, 46(20), 11,119–11,127. <https://doi.org/10.1021/es302558m>
- Fu, W., Randerson, J. T., & Keith Moore, J. (2016). Climate change impacts on net primary production (NPP) and export production (EP) regulated by increasing stratification and phytoplankton community structure in the CMIP5 models. *Biogeosciences*, 13(18), 5151–5170. <https://doi.org/10.5194/bg-13-5151-2016>
- Giglio, L., Randerson, J. T., Van Der Werf, G. R., Kasibhatla, P. S., Collatz, G. J., Morton, D. C., & DeFries, R. S. (2010). Assessing variability and long-term trends in burned area by merging multiple satellite fire products. *Biogeochemistry*, 97, 1171–1186.
- Ginoux, P., Prospero, J. M., Gill, T. E., Hsu, N. C., & Zhao, M. (2012). Global-scale attribution of anthropogenic and natural dust sources and their emission rates based on MODIS Deep Blue aerosol products. *Reviews of Geophysics*, 50, RG3005. <https://doi.org/10.1029/2012RG000388>
- Ginoux, P., Prospero, J. M., Torres, O., & Chin, M. (2004). Long-term simulation of global dust distribution with the GOCART model: Correlation with North Atlantic Oscillation. *Environmental Modelling and Software*, 19(2), 113–128. [https://doi.org/10.1016/S1364-8152\(03\)00114-2](https://doi.org/10.1016/S1364-8152(03)00114-2)
- Guieu, C., Aumont, O., Paytan, A., Bopp, L., Law, C. S., Mahowald, N., et al. (2014). Global biogeochemical cycles deposition to low nutrient low chlorophyll regions. *Global Biogeochemical Cycles*, 28, 1179–1198. <https://doi.org/10.1002/2014GB004852>
- Guieu, C., Bonnet, S., Wagener, T., & Loÿe-Pilot, M. D. (2005). Biomass burning as a source of dissolved iron to the open ocean? *Geophysical Research Letters*, 32, L19608. <https://doi.org/10.1029/2005GL022962>
- Hajima, T., Watanabe, M., Yamamoto, A., Tatebe, H., Noguchi, A., Abe, M., et al. (2019). Description of the MIROC-ES2L Earth system model and evaluation of its climate—Biogeochemical processes and feedbacks. *Geoscientific Model Development Discussion*, 5.
- Hamilton, D. S., Hantson, S., Scott, C. E., Kaplan, J. O., Pringle, K. J., Nieradzik, L. P., et al. (2018). Reassessment of pre-industrial fire emissions strongly affects anthropogenic aerosol forcing. *Nature Communications*, 9(1). <https://doi.org/10.1038/s41467-018-05592-9>
- Hamilton, D. S., Scanza, R. A., Feng, Y., Guinness, J., Kok, J. F., Li, L., et al. (2019). Improved methodologies for Earth system modelling of atmospheric soluble iron and observation comparisons using the Mechanism of Intermediate complexity for Modelling Iron (MIMI v1.0). *Geoscientific Model Development*, 12(9), 3835–3862. <https://doi.org/10.5194/gmd-12-3835-2019>
- Hand, J. L., Mahowald, N. M., Chen, Y., Siefert, R. L., Luo, C., Subramaniam, A., & Fung, I. (2004). Estimates of atmospheric-processed soluble iron from observations and a global mineral aerosol model: Biogeochemical implications. *Journal of Geophysical Research*, 109, D17205. <https://doi.org/10.1029/2004JD004574>
- Hantson, S., Lasslop, G., Kloster, S., & Chuvieco, E. (2015). Anthropogenic effects on global mean fire size. *International Journal of Wildland Fire*, 24(5), 589–596. <https://doi.org/10.1071/WF14208>
- Honeyman, B. D., Ballistrieri, L. S., & Murray, J. W. (1988). Oceanic trace metal scavenging: The importance of particle concentration. *Deep-Sea Research Part I: Oceanographic Research Papers*, 35(2), 227–246. [https://doi.org/10.1016/0198-0149\(88\)90038-6](https://doi.org/10.1016/0198-0149(88)90038-6)
- Hurrell, J. W., Holland, M. M., Gent, P. R., Ghan, S., Kay, J. E., Kushner, P. J., et al. (2013). The community Earth system model: A framework for collaborative research. *Bulletin of the American Meteorological Society*, 94(9). <https://doi.org/10.1175/BAMS-D-12-00121.1>
- Hutchins, D. A., & Boyd, P. W. (2016). Marine phytoplankton and the changing ocean iron cycle. *Nature Climate Change*, 6(12), 1072–1079. <https://doi.org/10.1038/nclimate3147>
- Ito, A. (2011). Mega fire emissions in Siberia: Potential supply of bioavailable iron from forests to the ocean. *Biogeosciences*, 8(6), 1679–1697. <https://doi.org/10.5194/bg-8-1679-2011>
- Ito, A. (2013). Global modeling study of potentially bioavailable iron input from shipboard aerosol sources to the ocean. *Global Biogeochemical Cycles*, 27, 1–10. <https://doi.org/10.1029/2012GB004378>
- Ito, A. (2015). Atmospheric processing of combustion aerosols as a source of bioavailable iron. *Environmental Science & Technology Letters*, 2(3), 70–75. <https://doi.org/10.1021/acs.estlett.5b00007>
- Ito, A., Myriokefalitakis, S., Kanakidou, M., Mahowald, N. M., Scanza, R. A., Hamilton, D. S., et al. (2019). Pyrogenic iron: The missing link to high iron solubility in aerosols. *Science Advances*, 5(5), eaau7671. <https://doi.org/10.1126/sciadv.aau7671>
- Ito, A., & Penner, J. E. (2005). Historical emissions of carbonaceous aerosols from biomass and fossil fuel burning for the period 1870–2000. *Global Biogeochemical Cycles*, 19(2), GB2028. <https://doi.org/10.1029/2004GB002374>

- Ito, A., & Shi, Z. (2016). Delivery of anthropogenic bioavailable iron from mineral dust and combustion aerosols to the ocean. *Atmospheric Chemistry and Physics*, 16(1), 85–99. <https://doi.org/10.5194/acp-16-85-2016>
- Ito, A., Lin, G., & Penner, J. E. (2018). Radiative forcing by light-absorbing aerosols of pyrogenic iron oxides. *Scientific Reports*, 8(1), 1–11. <https://doi.org/10.1038/s41598-018-25756-3>
- Ito, A., & Xu, L. (2014). Response of acid mobilization of iron-containing mineral dust to improvement of air quality projected in the future. *Atmospheric Chemistry and Physics*, 14(7), 3441–3459. <https://doi.org/10.5194/acp-14-3441-2014>
- Ito, A., Ye, Y., Yamamoto, A., Watanabe, M., & Aita, M. N. (2020). Responses of ocean biogeochemistry to atmospheric supply of lithogenic and pyrogenic iron-containing aerosols. *Geological Magazine*, 1–16. <https://doi.org/10.1017/S0016756819001080>
- Jannasch, H. W., Honeyman, B. D., & Murray, J. W. (1996). Marine scavenging: The relative importance of mass transfer and reaction rates. *Limnology and Oceanography*, 41(1), 82–88. <https://doi.org/10.4319/lo.1996.41.1.0082>
- Jayaratne, T., Stockwell, C. E., Bhave, P. V., Praveen, P. S., Rathnayake, C. M., Islam, M. R., et al. (2018). Nepal Ambient Monitoring and Source Testing Experiment (NAMaSTE): Emissions of particulate matter from wood- and dung-fueled cooking fires, garbage and crop residue burning, brick kilns, and other sources. *Atmospheric Chemistry and Physics*, 18(3), 2259–2286. <https://doi.org/10.5194/acp-18-2259-2018>
- Jickells, T. D., An, Z. S., Andersen, K. K., Baker, A. R., Bergametti, G., Brooks, N., et al. (2005). Global iron connections between desert dust, ocean biogeochemistry, and climate. *Science*, 308(5718), 67–71. <https://doi.org/10.1126/science.1105959>
- Johnson, M. S., & Meskhidze, N. (2013). Atmospheric dissolved iron deposition to the global oceans: Effects of oxalate-promoted Fe dissolution, photochemical redox cycling, and dust mineralogy. *Geoscientific Model Development*, 6(4), 1137–1155. <https://doi.org/10.5194/gmd-6-1137-2013>
- Jordi, A., Basterretxea, G., Tovar-Sánchez, A., Alastuey, A., & Querol, X. (2012). Copper aerosols inhibit phytoplankton growth in the Mediterranean Sea. *Proceedings of the National Academy of Sciences of the United States of America*, 109(52), 21,246–21,249. <https://doi.org/10.1073/pnas.1207567110>
- Journeet, E., Desboeufs, K. V., Caquineau, S., & Colin, J. L. (2008). Mineralogy as a critical factor of dust iron solubility. *Geophysical Research Letters*, 35, L07805. <https://doi.org/10.1029/2007GL031589>
- Kaplan, J. O., Bigelow, N. H., Prentice, I. C., Harrison, S. P., Bartlein, P. J., Christensen, T. R., et al. (2003). Climate change and Arctic ecosystems: And future projections. *Climate Dynamics*, 108, D19. <https://doi.org/10.1029/2002JD002559>
- King, A. L., Sañudo-Wilhelmy, S. A., Boyd, P. W., Twining, B. S., Wilhelm, S. W., Breene, C., et al. (2012). A comparison of biogenic iron quotas during a diatom spring bloom using multiple approaches. *Biogeosciences*, 9(2), 667–687. <https://doi.org/10.5194/bg-9-667-2012>
- Kleeman, M. J., Schauer, J. J., & Cass, G. R. (1999). Size and composition distribution of fine particulate matter emitted from wood burning, meat charbroiling, and cigarettes. *Environmental Science & Technology*, 33(20), 3516–3523. <https://doi.org/10.1021/es981277q>
- Klein Goldewijk, K., Beusen, A., Doelman, J., & Stehfest, E. (2017). New anthropogenic land use estimates for the Holocene; HYDE 3.2. *Earth System Science Data Discussions*, 927–953. <https://doi.org/10.5194/essd-9-927-2017>
- Kloster, S., Mahowald, N., Randerson, J., & Lawrence, P. (2012a). Future fire emissions simulated within the CLM-CN. *Biogeosciences*, 9, 509–525.
- Kloster, S., Mahowald, N. M., Randerson, J. T., & Lawrence, P. J. (2012b). The impacts of climate, land use, and demography on fires during the 21st century simulated by CLM-CN. *Biogeosciences*, 9(1), 509–525. <https://doi.org/10.5194/bg-9-509-2012>
- Knorr, W., Jiang, L., & Arneth, A. (2016). Climate, CO<sub>2</sub> and human population impacts on global wildfire emissions. *Biogeosciences*, 13(1), 267–282. <https://doi.org/10.5194/bg-13-267-2016>
- Knorr, W., Kaminski, T., Arneth, A., & Weber, U. (2014). Impact of human population density on fire frequency at the global scale. *Biogeosciences*, 11(4), 1085–1102. <https://doi.org/10.5194/bg-11-1085-2014>
- Kohfeld, K. E., & Ridgwell, A. (2009). Glacial-interglacial variability in atmospheric CO<sub>2</sub>. In *Surface Ocean–Lower Atmosphere Processes, Geophysical Research Series* (pp. 251–286). Washington, D. C: American Geophysical Union.
- Kok, J. F. (2011). A scaling theory for the size distribution of emitted dust aerosols suggests climate models underestimate the size of the global dust cycle. *Proceedings of the National Academy of Sciences*, 108(3), 1016–1021. <https://doi.org/10.1073/pnas.1014798108>
- Kok, J. F., Albani, S., Mahowald, N. M., & Ward, D. S. (2014). An improved dust emission model—Part 2: Evaluation in the Community Earth System Model, with implications for the use of dust source functions. *Atmospheric Chemistry and Physics*, 14(23), 13,043–13,061. <https://doi.org/10.5194/acp-14-13043-2014>
- Kok, J. F., Ward, D. S., Mahowald, N. M., & Evan, A. T. (2018). Global and regional importance of the direct dust-climate feedback. *Nature Communications*, 9(1). <https://doi.org/10.1038/s41467-017-02620-y>
- Krishnamurthy, A., Moore, J. K., Mahowald, N., Luo, C., Doney, S. C., Lindsay, K., & Bender, C. S. (2009). Impacts of increasing anthropogenic soluble iron and nitrogen deposition on ocean biogeochemistry. *Global Biogeochemical Cycles*, 23, GB3016. <https://doi.org/10.1029/2008GB003440>
- Lamarque, J.-F., Bond, T. C., Eyring, V., Granier, C., Heil, A., Klimont, Z., et al. (2010). Historical (1850–2000) gridded anthropogenic and biomass burning emissions of reactive gases and aerosols: Methodology and application. *Atmospheric Chemistry and Physics*, 10(15), 7017–7039. <https://doi.org/10.5194/acp-10-7017-2010>
- Lancelot, C., De Montety, A., Goosse, H., Becquevert, S., Schoemann, V., Pasquer, B., & Vancoppenolle, M. (2009). Spatial distribution of the iron supply to phytoplankton in the Southern Ocean: A model study. *Biogeosciences*, 6(12), 2861–2878. <https://doi.org/10.5194/bg-6-2861-2009>
- Li, F., Val Martin, M., Hantson, S., Andreae, M. O., Arneth, A., Lasslop, G., et al. (2019). Historical (1700–2012) global multi-model estimates of the fire emissions from the Fire Modeling Intercomparison Project (FireMIP). *Atmospheric Chemistry and Physics Discussions*, 1–57. <https://doi.org/10.5194/acp-2019-37>
- Li, W., Xu, L., Liu, X., Zhang, J., Lin, Y., Yao, X., et al. (2017). Air pollution–aerosol interactions produce more bioavailable iron for ocean ecosystems. *Science Advances*, 1–7. <https://doi.org/10.1126/sciadv.1601749>
- Li, X., Wang, S., Duan, L., Hao, J., & Nie, Y. (2009). Carbonaceous aerosol emissions from household biofuel combustion in China. *Environmental Science & Technology*, 43(15), 6076–6081. <https://doi.org/10.1021/es803330j>
- Luo, C., Mahowald, N., Bond, T., Chuang, P. Y., Artaxo, P., Siefert, R., et al. (2008). Combustion iron distribution and deposition. *Global Biogeochemical Cycles*, 22, GB1012. <https://doi.org/10.1029/2007GB002964>
- Luo, C., Mahowald, N. M., & Corral, J. (2003). Sensitivity study of meteorological parameters on mineral aerosol mobilization, transport, and distribution. *Journal of Geophysical Research*, 108(D15), 4447. <https://doi.org/10.1029/2003JD003483>
- Mackey, K. R. M., Post, A. F., McIlvin, M. R., Cutter, G. A., John, S. G., Saito, M. A., & Haselkorn, R. (2015). Divergent responses of Atlantic coastal and oceanic *Synechococcus* to iron limitation. *Proceedings of the National Academy of Sciences of the United States of America*, 112(32), 9944–9949. <https://doi.org/10.1073/pnas.1509448112>

- Mahowald, N., Lindsay, K., Rothenberg, D., Doney, S. C., Moore, J. K., Thornton, P., et al. (2011). Desert dust and anthropogenic aerosol interactions in the Community Climate System Model coupled-carbon-climate model. *Biogeosciences*, 8(2), 387–414. <https://doi.org/10.5194/bg-8-387-2011>
- Mahowald, N., Ward, D. S., Kloster, S., Flanner, M. G., Heald, C. L., Heavens, N. G., et al. (2011). Aerosol impacts on climate and biogeochemistry. *Annual Review of Environment and Resources*, 36(1), 45–74. <https://doi.org/10.1146/annurev-environ-042009-094507>
- Mahowald, N. M. (2007). Anthropocene changes in desert area: Sensitivity to climate model predictions. *Geophysical Research Letters*, 34, L18817. <https://doi.org/10.1029/2007GL030472>
- Mahowald, N. M., Engelstaedter, S., Luo, C., Sealy, A., Artaxo, P., Benitez-Nelson, C., et al. (2009). Atmospheric iron deposition: Global distribution, variability, and human perturbations. *Annual Review of Marine Science*, 1, 245–278. <https://doi.org/10.1146/annurev-marine.010908.163727>
- Mahowald, N. M., Hamilton, D. S., Mackey, K. R. M., Moore, J. K., Baker, A. R., Scanza, R. A., & Zhang, Y. (2018). Aerosol trace metal leaching and impacts on marine microorganisms. *Nature Communications*, 9(1), 2614. <https://doi.org/10.1038/s41467-018-04970-7>
- Mahowald, N. M., Kloster, S., Engelstaedter, S., Moore, J. K., Mukhopadhyay, S., McConnell, J. R., et al. (2010). Observed 20th century desert dust variability: Impact on climate and biogeochemistry. *Atmospheric Chemistry and Physics*, 10(22), 10,875–10,893. <https://doi.org/10.5194/acp-10-10875-2010>
- Mallek, C., Safford, H., Viers, J., & Miller, J. (2013). Modern departures in fire severity and area vary by forest type, Sierra Nevada and southern Cascades, California, USA. *Ecosphere*, 4(12), 1–28. <https://doi.org/10.1890/ES13-00217.1>
- Marinov, I., Gnanadesikan, A., Toggweiler, J. R., & Sarmiento, J. L. (2006). The Southern Ocean biogeochemical divide. *Nature*, 441(7096), 964–967. <https://doi.org/10.1038/nature04883>
- Martin, H., Gordon, R. M., & Fitzwater, S. E. (1991). The case for iron. *Limnology and Oceanography*, 36(8), 1793–1802.
- Martin, J. (1990). Glacial-interglacial CO<sub>2</sub> change: The iron hypothesis. *Paleoceanography*, 5(1), 1–13.
- Martiny, A. C., Lomas, M. W., Fu, W., Boyd, P. W., Chen, Y. L., Cutter, G. A., et al. (2019). Biogeochemical controls of surface ocean phosphate. *Science Advances*, 5(8), eaax0341. <https://doi.org/10.1126/sciadv.aax0341>
- Martiny, A. C., Pham, C. T. A., Primeau, F. W., Vrugt, J. A., Moore, J. K., Levin, S. A., & Lomas, M. W. (2013). Strong latitudinal patterns in the elemental ratios of marine plankton and organic matter. *Nature Geoscience*, 6(4), 279–283. <https://doi.org/10.1038/ngeo1757>
- Matsui, H., Mahowald, N. M., Moteki, N., Hamilton, D. S., Ohata, S., Yoshida, A., et al. (2018). Anthropogenic combustion iron as a complex climate forcer. *Nature Communications*, 9(1), 1593. <https://doi.org/10.1038/s41467-018-03997-0>
- McConnell, J. R., Aristarain, A. J., Banta, J. R., Edwards, P. R., & Simo, J. C. (2007). 20th-Century doubling in dust archived in an Antarctic Peninsula ice core parallels climate change and desertification in South America. *Proceedings of the National Academy of Sciences of the United States of America*, 104(14), 5743–5748. <https://doi.org/10.1073/pnas.0607657104>
- Meskhidze, N., Chameides, W. L., Nenes, A., & Chen, G. (2003). Iron mobilization in mineral dust: Can anthropogenic SO<sub>2</sub> emissions affect ocean productivity? *Geophysical Research Letters*, 30(21), 2085. <https://doi.org/10.1029/2003GL018035>
- Meskhidze, N., Völker, C., Al-Abadleh, H. A., Barbeau, K., Bressac, M., Buck, C., et al. (2019). Perspective on identifying and characterizing the processes controlling iron speciation and residence time at the atmosphere-ocean interface. *Marine Chemistry*, 217, 103704. <https://doi.org/10.1016/j.marchem.2019.103704>
- Mitchell, R. S., & Gluskoter, H. J. (1976). Mineralogy of ash of some American coals: Variations with temperature and source. *Fuel*, 55(2), 90–96. [https://doi.org/10.1016/0016-2361\(76\)90001-6](https://doi.org/10.1016/0016-2361(76)90001-6)
- Moore, C. M. M., Mills, M. M. M., Arrigo, K. R. R., Berman-Frank, I., Bopp, L., Boyd, P. W. W., et al. (2013). Processes and patterns of oceanic nutrient limitation. *Nature Geoscience*, 6(9), 701–710. <https://doi.org/10.1038/ngeo1765>
- Moore, J. K., & Braucher, O. (2008). Sedimentary and mineral dust sources of dissolved iron to the world ocean. *Biogeosciences*, 5(3), 631–656. <https://doi.org/10.5194/bg-5-631-2008>
- Moore, J. K., Doney, S. C., & Lindsay, K. (2004). Upper ocean ecosystem dynamics and iron cycling in a global three-dimensional model. *Global Biogeochemical Cycles*, 18, GB4028. <https://doi.org/10.1029/2004GB002220>
- Moore, J. K., Fu, W., Primeau, F., Britten, G. L., Lindsay, K., Long, M., et al. (2018). Sustained climate warming drives declining marine biological productivity. *Science*, 359(6380), 113–1143. <https://doi.org/10.1126/science.aa06379>
- Moore, J. K., Lindsay, K., Doney, S. C., Long, M. C., & Misumi, K. (2013). Marine ecosystem dynamics and biogeochemical cycling in the community Earth system model [CESM1(BGC)]: Comparison of the 1990s with the 2090s under the RCP4.5 and RCP8.5 scenarios. *Journal of Climate*, 26(23), 9291–9312. <https://doi.org/10.1175/JCLI-D-12-00566.1>
- Moore, K., Doney, S. C., Lindsay, K., Mahowald, N., & Michaels, A. F. (2006). Nitrogen fixation amplifies the ocean biogeochemical response to decadal timescale variations in mineral dust deposition. *Tellus Series B: Chemical and Physical Meteorology*, 58(5), 560–572. <https://doi.org/10.1111/j.1600-0889.2006.00209.x>
- Morel, F. M. M., & Price, N. M. (2003). The biogeochemical cycles of trace metals in the oceans. *Science*, 300(5621), 944–947. <https://doi.org/10.1126/science.1083545>
- Mulitz, S., Heslop, D., Pittauerova, D., Fischer, H. W., Meyer, I., Stuut, J. B., et al. (2010). Increase in African dust flux at the onset of commercial agriculture in the Sahel region. *Nature*, 466(7303), 226–228. <https://doi.org/10.1038/nature09213>
- Myriokefalitakis, S., Ito, A., Kanakidou, M., Nenes, A., Krol, M. C., Mahowald, N. M., et al. (2018). Reviews and syntheses: The GESAMP atmospheric iron deposition modelintercomparison study. *Biogeosciences*, 15(21), 6659–6684. <https://doi.org/10.5194/bg-15-6659-2018>
- Myriokefalitakis, S., Daskalakis, N., Mihalopoulos, N., Baker, A. R., Nenes, A., & Kanakidou, M. (2015). Changes in dissolved iron deposition to the oceans driven by human activity: A 3-D global modelling study. *Biogeosciences*, 12(13), 3973–3992. <https://doi.org/10.5194/bg-12-3973-2015>
- Myriokefalitakis, S., Tsigaridis, K., Mihalopoulos, N., Sciare, J., Nenes, A., Kawamura, K., et al. (2011). In-cloud oxalate formation in the global troposphere: A 3-D modeling study. *Atmospheric Chemistry and Physics*, 11(12), 5761–5782. <https://doi.org/10.5194/acp-11-5761-2011>
- Namdari, S., Karimi, N., Sorooshian, A., Mohammadi, G. H., & Sehatkashani, S. (2018). Impacts of climate and synoptic fluctuations on dust storm activity over the Middle East. *Atmospheric Environment*, 173(November 2017), 265–276. <https://doi.org/10.1016/j.atmosenv.2017.11.016>
- Neff, J. C., Ballantyne, A. P., Farmer, G. L., Mahowald, N. M., Conroy, J. L., Landry, C. C., et al. (2008). Increasing eolian dust deposition in the western United States linked to human activity. *Nature Geoscience*, 1(3), 189–195. <https://doi.org/10.1038/ngeo133>
- Oakes, M., Ingall, E. D., Lai, B., Shafer, M. M., Hays, M. D., Liu, Z. G., et al. (2012). Iron solubility related to particle sulfur content in source emission and ambient fine particles. *Environmental Science & Technology*, 46(12), 6637–6644. <https://doi.org/10.1021/es300701c>

- Olgun, N., Duggen, S., Croot, P. L., Delmelle, P., Dietze, H., Schacht, U., et al. (2011). Surface ocean iron fertilization: The role of airborne volcanic ash from subduction zone and hot spot volcanoes and related iron fluxes into the Pacific Ocean. *Global Biogeochemical Cycles*, 25, GB4001. <https://doi.org/10.1029/2009GB003761>
- Pacyna, J. M., & Pacyna, E. G. (2001). An assessment of global and regional emissions of trace metals to the atmosphere from anthropogenic sources worldwide. *Environmental Reviews*, 9(4), 269–298. <https://doi.org/10.1139/er-9-4-269>
- Parekh, P., Follows, M. J., & Boyle, E. (2004). Modeling the global ocean iron cycle. *Global Biogeochemical Cycles*, 18, GB1002. <https://doi.org/10.1029/2003GB002061>
- Paris, R., Desboeufs, K. V., Formenti, P., Nava, S., & Chou, C. (2010). Chemical characterisation of iron in dust and biomass burning aerosols during AMMA-SOP0/DABEX: Implication for iron solubility. *Atmospheric Chemistry and Physics*, 10(9), 4273–4282. <https://doi.org/10.5194/acp-10-4273-2010>
- Paytan, A., Mackeya, K. R. M., Chena, Y., Limac, I. D., Doney, S. C. S. C., Mahowald, N., et al. (2009). Toxicity of atmospheric aerosols on marine phytoplankton. *Proceedings of the National Academy of Sciences of the United States of America*, 106(12), 4601–4605. <https://doi.org/10.1073/pnas.0811486106>
- Pechony, O., & Shindell, D. T. (2010). Driving forces of global wildfires over the past millennium and the forthcoming century. *Proceedings of the National Academy of Sciences*, 107(45), 19,167–19,170. <https://doi.org/10.1073/pnas.1003669107>
- Pfeiffer, M., Spessa, A., & Kaplan, J. O. (2013). A model for global biomass burning in preindustrial time: LPJ-LMfire (v1.0). *Geoscientific Model Development*, 6(3), 643–685. <https://doi.org/10.5194/gmd-6-643-2013>
- Rabin, S. S., Melton, J. R., Lasslop, G., Bachelet, D., Forrest, M., Hantson, S., et al. (2017). The Fire Modeling Intercomparison Project (FireMIP), phase 1: Experimental and analytical protocols with detailed model descriptions. *Geoscientific Model Development*, 10(3), 1175–1197. <https://doi.org/10.5194/gmd-10-1175-2017>
- Rauch, J. N., & Pacyna, J. M. (2009). Earth's global Ag, Al, Cr, Cu, Fe, Ni, Pb, and Zn cycles. *Global Biogeochemical Cycles*, 23, GB2001. <https://doi.org/10.1029/2008GB003376>
- Rienecker, M. M., Suarez, M. J., Todling, R., Bacmeister, J., Takacs, L., Liu, H.-C., et al. (2008). The GEOS-5 Data Assimilation System—Documentation of versions 5.0.1, 5.1.0, and 5.2.0.
- Scanza, R. A., Hamilton, D. S., Perez Garcia-Pando, C., Buck, C., Baker, A., & Mahowald, N. M. (2018). Atmospheric processing of iron in mineral and combustion aerosols: Development of an intermediate-complexity mechanism suitable for Earth system models. *Atmospheric Chemistry and Physics*, 18(19), 14,175–14,196. <https://doi.org/10.5194/acp-18-14175-2018>
- Scanza, R. A., Mahowald, N., Ghan, S., Zender, C. S., Kok, J. F., Liu, X., et al. (2015). Modeling dust as component minerals in the Community Atmosphere Model: Development of framework and impact on radiative forcing. *Atmospheric Chemistry and Physics*, 15(1), 537–561. <https://doi.org/10.5194/acp-15-537-2015>
- Schmidl, C., Marr, I. L., Caseiro, A., Kotianová, P., Berner, A., Bauer, H., et al. (2008). Chemical characterisation of fine particle emissions from wood stove combustion of common woods growing in mid-European Alpine regions. *Atmospheric Environment*, 42(1), 126–141. <https://doi.org/10.1016/j.atmosenv.2007.09.028>
- Schroth, A. W., Crusius, J., Sholkovitz, E. R., & Bostick, B. C. (2009). Iron solubility driven by speciation in dust sources to the ocean. *Nature Geoscience*, 2(5), 337–340. <https://doi.org/10.1038/ngeo501>
- Sedwick, P. N., Sholkovitz, E. R., & Church, T. M. (2007). Impact of anthropogenic combustion emissions on the fractional solubility of aerosol iron: Evidence from the Sargasso Sea. *Geochemistry, Geophysics, Geosystems*, 8, Q10Q06. <https://doi.org/10.1029/2007GC001586>
- Shi, Z., Krom, M. D., Bonneville, S., & Benning, L. G. (2015). Atmospheric processing outside clouds increases soluble iron in mineral dust. *Environmental Science & Technology*, 49(3), 1472–1477. <https://doi.org/10.1021/es504623x>
- Shi, Z., Krom, M. D., Jickells, T. D., Bonneville, S., Carslaw, K. S., Mihalopoulos, N., et al. (2012). Impacts on iron solubility in the mineral dust by processes in the source region and the atmosphere: A review. *Aeolian Research*, 5(May), 21–42. <https://doi.org/10.1016/j.aeolia.2012.03.001>
- Sholkovitz, E. R., Sedwick, P. N., Church, T. M., Baker, A. R., & Powell, C. F. (2012). Fractional solubility of aerosol iron: Synthesis of a global-scale data set. *Geochimica et Cosmochimica Acta*, 89, 173–189. <https://doi.org/10.1016/j.gca.2012.04.022>
- Solomon, F., Chuang, P. Y., Meskhidze, N., & Chen, Y. (2009). Acidic processing of mineral dust iron by anthropogenic compounds over the north Pacific Ocean. *Journal of Geophysical Research*, 114, D02305. <https://doi.org/10.1029/2008JD010417>
- Stanelle, T., Bey, I., Raddatz, T., Reick, C., & Tegen, I. (2014). Anthropogenically induced changes in twentieth century mineral dust burden and the associated impact on radiative forcing. *Journal of Geophysical Research: Atmospheres*, 119, 13,526–13,546. <https://doi.org/10.1002/2014JD022062>
- Tagliabue, A., Aumont, O., DeAth, R., Dunne, J. P., Dutkiewicz, S., Galbraith, E., et al. (2016). How well do global ocean biogeochemistry models simulate dissolved iron distributions? *Global Biogeochemical Cycles*, 30(2), 149–174. <https://doi.org/10.1002/2015GB005289>
- Tagliabue, A., Bopp, L., & Aumont, O. (2008). Ocean biogeochemistry exhibits contrasting responses to a large scale reduction in dust deposition. *Biogeosciences*, 5(1), 11–24. <https://doi.org/10.5194/bg-5-11-2008>
- Tagliabue, A., Bopp, L., Roche, D., Bouttes, N., Dutay, J.-C., Alkama, R., et al. (2009). Quantifying the roles of ocean circulation and biogeochemistry in governing ocean carbon-13 and atmospheric carbon dioxide at the last glacial maximum. *Climate of the Past*, 5, 695–706.
- Tagliabue, A., Bowie, A. R., Boyd, P. W., Buck, K. N., Johnson, K. S., & Saito, M. A. (2017). The integral role of iron in ocean biogeochemistry. *Nature*, 543(7643), 51–59. <https://doi.org/10.1038/nature21058>
- Tagliabue, A., Bowie, A. R., DeVries, T., Ellwood, M. J., Landing, W. M., Milne, A., et al. (2019). The interplay between regeneration and scavenging fluxes drives ocean iron cycling. *Nature Communications*, 10(1), 4960. <https://doi.org/10.1038/s41467-019-12775-5>
- Tagliabue, A., Mtshali, T., Aumont, O., Bowie, A. R., Klunder, M. B., Roychoudhury, A. N., & Swart, S. (2012). A global compilation of dissolved iron measurements: Focus on distributions and processes in the Southern Ocean. *Biogeosciences*, 9(6), 2333–2349. <https://doi.org/10.5194/bg-9-2333-2012>
- Tegen, I., Werner, M., Harrison, S. P., & Kohfeld, K. E. (2004). Relative importance of climate and land use in determining present and future global soil dust emission. *Geophysical Research Letters*, 31, L05105. <https://doi.org/10.1029/2003GL019216>
- Textor, C., Schulz, M., Guibert, S., Kinne, S., Balkanski, Y., Bauer, S., et al. (2006). Analysis and quantification of the diversities of aerosol life cycles within AeroCom. *Atmospheric Chemistry and Physics*, 6, 1777–1813. <https://doi.org/10.5194/acpd-5-8331-2005>
- Turnock, S. T., Spracklen, D. V., Carslaw, K. S., Mann, G. W., Woodhouse, M. T., Forster, P. M., et al. (2015). Modelled and observed changes in aerosols and surface solar radiation over Europe between 1960 and 2009. *Atmospheric Chemistry and Physics*, 15(16), 9477–9500. <https://doi.org/10.5194/acp-15-9477-2015>
- Twining, B. S., Baines, S. B., Bozard, J. B., Vogt, S., Walker, E. A., & Nelson, D. M. (2011). Metal quotas of plankton in the equatorial Pacific Ocean. *Deep-Sea Research Part II: Topical Studies in Oceanography*, 58(3–4), 325–341. <https://doi.org/10.1016/j.dsrr.2010.08.018>

- Veira, A., Lasslop, G., & Kloster, S. (2016). Wildfires in a warmer climate: Emission fluxes, emission heights, and black carbon concentrations in 2090–2099. *Journal of Geophysical Research: Atmospheres*, 121, 3195–3223. <https://doi.org/10.1002/2015JD024142>
- Wang, R., Balkanski, Y., Bopp, L., Aumont, O., Boucher, O., Caias, P., et al. (2015). Influence of anthropogenic aerosol deposition on the relationship between oceanic productivity and warming. *Geophysical Research Letters*, 42, 10,745–10,754. <https://doi.org/10.1002/2015GL066753>
- Wang, W. L., Moore, J. K., Martiny, A. C., & Primeau, F. W. (2019). Convergent estimates of marine nitrogen fixation. *Nature*, 566(7743), 205–211. <https://doi.org/10.1038/s41586-019-0911-2>
- Ward, D. S., Kloster, S., Mahowald, N. M., Rogers, B. M., Randerson, J. T., & Hess, P. G. (2012). The changing radiative forcing of fires: Global model estimates for past, present and future. *Atmospheric Chemistry and Physics*, 12(22), 10,857–10,886. <https://doi.org/10.5194/acp-12-10857-2012>
- Watanabe, M., Aita, M. N.-A., & Hajima, T. (2018). Development of a marine ecosystem model to be embedded into an Earth system model. *Oceanography in Japan*, 27(1), 31–41.
- Watson, J. G., & Chow, J. C. (2001). Source characterization of major emission sources in the Imperial and Mexicali Valleys along the US/Mexico border. *Science of the Total Environment*, 276(1–3), 33–47. [https://doi.org/10.1016/S0048-9697\(01\)00770-7](https://doi.org/10.1016/S0048-9697(01)00770-7)
- Weber, R. J., Guo, H., Russell, A. G., & Nenes, A. (2016). High aerosol acidity despite declining atmospheric sulfate concentrations over the past 15 years. *Nature Geoscience*, 9, 1–5. <https://doi.org/10.1038/NGEO2665>
- Wingenter, O. W., Haase, K. B., Strutton, P., Friederich, G., Meinardi, S., Blake, D. R., & Rowland, F. S. (2004). Changing concentrations of CO, CH<sub>4</sub>, C<sub>2</sub>H<sub>6</sub>, CH<sub>3</sub>Br, CH<sub>3</sub>I, and dimethyl sulfide during the Southern Ocean Iron Enrichment Experiments. *Proceedings of the National Academy of Sciences*, 101(23), 8537–8541. <https://doi.org/10.1073/pnas.0402744101>
- Winton, V. H. L., Bowie, A. R., Edwards, R., Keywood, M., Townsend, A. T., van der Merwe, P., & Bollhofer, A. (2015). Fractional iron solubility of atmospheric iron inputs to the Southern Ocean. *Marine Chemistry*, 177, 20–32. <https://doi.org/10.1016/j.marchem.2015.06.006>
- Woodward, S., Roberts, D. L., & Betts, R. A. (2005). A simulation of the effect of climate change-induced desertification on mineral dust aerosol. *Geophysical Research Letters*, 32, L18810. <https://doi.org/10.1029/2005GL023482>
- Wyatt, N. J., Milne, A., Woodward, E. M. S., Rees, A. P., Browning, T. J., Bouman, H. A., et al. (2014). Biogeochemical cycling of dissolved zinc along the GEOTRACES South Atlantic transect GA10 at 40°S. *Global Biogeochemical Cycles*, 28, 44–56. <https://doi.org/10.1002/2013GB004637>
- Ye, Y., & Völker, C. (2017). On the role of dust-deposited lithogenic particles for iron cycling in the tropical and subtropical Atlantic. *Global Biogeochemical Cycles*, 31, 1543–1558. <https://doi.org/10.1002/2017GB005663>
- Yoshioka, M., Mahowald, N., Dufresne, J. L., & Lou, C. (2005). Simulation of absorbing aerosol indices for African dust. *Journal of Geophysical Research*, 110, D18S17. <https://doi.org/10.1029/2004JD005276>
- Zender, C. S. (2003). Mineral Dust Entrainment and Deposition (DEAD) model: Description and 1990s dust climatology. *Journal of Geophysical Research*, 108(D14), 4416. <https://doi.org/10.1029/2002JD002775>
- Zhang, C., Ito, A., Shi, Z., Aita, M. N., Yao, X., Chu, Q., et al. (2019). Fertilization of the Northwest Pacific Ocean by East Asia air pollutants. *Global Biogeochemical Cycles*, 33, 690–702. <https://doi.org/10.1029/2018GB006146>
- Zhang, H., Wang, S., Hao, J., Wan, L., Jiang, J., Zhang, M., et al. (2012). Chemical and size characterization of particles emitted from the burning of coal and wood in rural households in Guizhou, China. *Atmospheric Environment*, 51, 94–99. <https://doi.org/10.1016/j.atmosenv.2012.01.042>
- Zhang, Y., Mahowald, N., Scanza, R. A., Journet, E., Desboeufs, K., Albani, S., et al. (2015). Modeling the global emission, transport and deposition of trace elements associated with mineral dust. *Biogeosciences*, 12(19), 5771–5792. <https://doi.org/10.5194/bg-12-5771-2015>